AD-A071 811 AEROSPACE CORP EL SEGUNDO CA AEROPHYSICS LAB F/G 16/1
A SHOCK TUBE INVESTIGATION OF SILO-LAUNCHED VEHICLE AERODYNAMIC--ETC(U)
JUL 79 R L VARWIG, D H ROSS, J M LYONS F04701-78-C-0079
UNCLASSIFIED TR-0079(4550-83)-1 SAMSO-TR-79-48 NL

| OF |
AD
A071811

END
DATE
FILMED
8-79
DDC

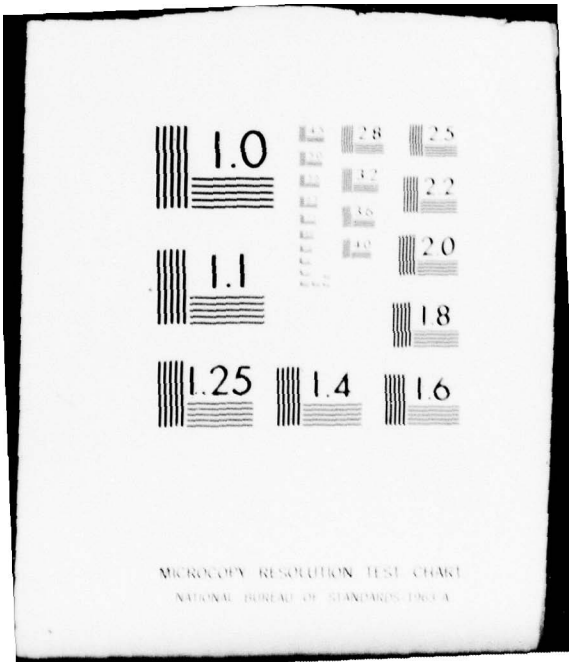
1.0
1.1
1.25
1.4
1.6
2.8
2.5
3.2
2.2
3.6
2.0
1.8
MICROCOPY RESOLUTION TEST CHART
NATIONAL BUREAU OF STANDARDS-1963-A

REPORT SAMSO-TR-79-48

LEVEL II

12

A Shock Tube Investigation of Silo-Launched Vehicle Aerodynamic Flow Asymmetries

R. L. VARWIG and D. H. ROSS
Aerophysics Laboratory
The Aerospace Corporation
El Segundo, Calif. 90245
and
J. M. LYONS
R&D Associates
Albuquerque N. Mex. 87117

5 July 1979

Interim Report

Prepared for
SPACE AND MISSILE SYSTEMS ORGANIZATION
AIR FORCE SYSTEMS COMMAND
Los Angeles Air Force Station
P.O. Box 92960, Worldway Postal Center
Los Angeles, Calif. 90009

This interim report was submitted by The Aerospace Corporation, El Segundo, CA 90245, under Contract No. F04701-78-C-0079 with the Space and Missile Systems Organization, Deputy for Advanced Space Programs, P. O. Box 92960, Worldway Postal Center, Los Angeles, CA 90009. It was reviewed and approved for The Aerospace Corporation by R. E. Clauser, Principal Director, Flight Test Support, Reentry Systems Division. Major B. F. Eakle, SAMSO/RSTPI, was the project officer for Reentry Systems.

This report has been reviewed by the Information Office (OI) and is releasable to the National Technical Information Service (NTIS). At NTIS, it will be available to the general public, including foreign nations.

This technical report has been reviewed and is approved for publication. Publication of this report does not constitute Air Force approval of the report's findings or conclusions. It is published only for the exchange and stimulation of ideas.

Bruce F. Eakle, Maj, USAF
Project Officer

Horace D. Smith, Lt Col, USAF
Chief, Flight Test Planning and Operations Division

FOR THE COMMANDER

Lloyd R. Norris, Col, USAF
Deputy for Technology

UNCLASSIFIED

SECURITY CLASSIFICATION OF THIS PAGE (When Data Entered)

REPORT DOCUMENTATION PAGE	READ INSTRUCTIONS BEFORE COMPLETING FORM
1. REPORT NUMBER: SAMSO-TR-79-48	2. GOVT ACCESSION NO.
3. RECIPIENT'S CATALOG NUMBER	
4. TITLE (and Subtitle): A SHOCK TUBE INVESTIGATION OF SILO-LAUNCHED VEHICLE AERODYNAMIC FLOW ASYMMETRIES	5. TYPE OF REPORT & PERIOD COVERED: Interim rept.
6. PERFORMING ORG. REPORT NUMBER: TR-0079(4550-83)-1	
7. AUTHOR(s): Robert L. Varwig, David H. Ross, and J. M. Lyons (R&D Associates)	8. CONTRACT OR GRANT NUMBER(s): F04701-78-C-0079
9. PERFORMING ORGANIZATION NAME AND ADDRESS: The Aerospace Corporation, El Segundo, Calif. 90245	10. PROGRAM ELEMENT, PROJECT, TASK AREA & WORK UNIT NUMBERS: 59p.
11. CONTROLLING OFFICE NAME AND ADDRESS: Space and Missile Systems Organization, Air Force Systems Command, Los Angeles, Calif. 90009	12. REPORT DATE: 5 July 1979
	13. NUMBER OF PAGES: 55
14. MONITORING AGENCY NAME & ADDRESS (if different from Controlling Office)	15. SECURITY CLASS. (of this report): Unclassified
	15a. DECLASSIFICATION/DOWNGRADING SCHEDULE

16. DISTRIBUTION STATEMENT (of this Report)

Approved for public release; distribution unlimited

17. DISTRIBUTION STATEMENT (of the abstract entered in Block 20, if different from Report)

18. SUPPLEMENTARY NOTES

19. KEY WORDS (Continue on reverse side if necessary and identify by block number)

Shock Tube
Silo Launch Vehicles
Pressure Transducers

20. ABSTRACT (Continue on reverse side if necessary and identify by block number)

A shock tube was used to simulate the initial transient flow from a rocket launching silo when the rocket motor was ignited. The object was to investigate the relationship between lateral loads observed on the missile being launched during the early transient flow and the silo exit geometry. A centerbody simulating the missile to be launched was installed in the shock tube and instrumented with pressure gages to detect the lateral loads. Three silo exit geometries were also modeled. The early transient flow

DD FORM 1473 (FACSIMILE)

UNCLASSIFIED

SECURITY CLASSIFICATION OF THIS PAGE (When Data Entered)

409 367

19. KEY WORDS (Continued)

20. ABSTRACT (Continued)

in the silo is described along with the modeling of this flow by the shock tube. Finally, the pressures measured on the missile model are presented together with a correlation technique that was developed to display the effect of the silo exit geometries on the model pressure difference force. Also included are results from the application of this correlation technique to full-scale flight data, which appear to demonstrate a close relationship between on-board accelerometer measurements and the pressure difference force history.

PREFACE

We wish to acknowledge the work of Terry Felker and John Nakamura in constructing the instrumentation and conducting the tests, and the work of Kenneth Glaser and Frances Twillie in programming the digital filtering, coordinate transformations, and output plots required for this task. In addition, the advice and support of Dr. Harold Mirels are acknowledged.

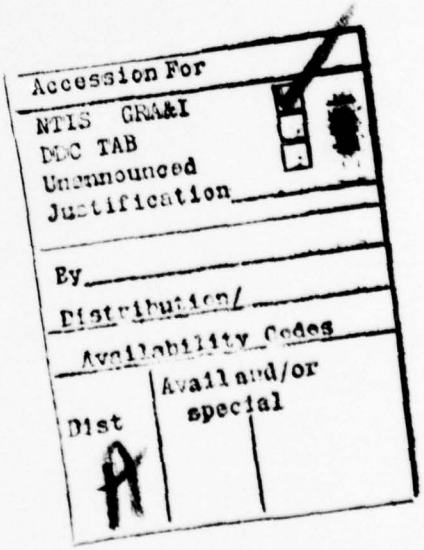

CONTENTS

FIGURES

FIGURES (Continued)

I. INTRODUCTION

Large lateral payload accelerations have been observed during launch of Minuteman vehicles employed for research studies. Several explanations of the cause of these accelerations have been offered. One theory is that flow separation in the rocket exhaust nozzle, during startup, causes large lateral loads that are transmitted to the payload. A second theory is that the lateral payload accelerations are due to aerodynamic forces associated with silo exit asymmetries.

Minuteman vehicles employed on research missions are launched from shallow silos with the upper third of the vehicle initially projective from the silo. In this configuration protection from weather prior to launch is afforded by a light but sturdy styrofoam structure. On ignition of the rocket motor the initial transient flow from the silo is expected to destroy the foam structure. However, limited pressure and acceleration measurements made on the vehicle have indicated that asymmetric aerodynamic loads exist on the vehicle. These asymmetric loads may be caused by the interaction of the initial transient flow with the expendable foam environmental structure before it disintegrates or by interaction with other asymmetrical features of the silo exit geometry.

As a means of examining the cause of the asymmetric loading, a laboratory experiment was performed in which a large-diameter shock tube served as the silo. A centerbody simulating the vehicle was mounted in the shock tube with the fore end projecting from the shock tube. Thus, the shock wave in the annular shock tube formed by the centerbody and the shock tube walls served as the initial transient flow in analogy to the flow in the full scale silo between the missile and the silo walls. In this experiment the forebody of the simulated vehicle was instrumented with pressure transducers. The geometry of the silo exit was duplicated, including the expendable shelter.

In this report the early transient flow in the silo is described following Broadwell and Tsu.[1] The modeling of the flow by the shock tube is discussed, and the experimental results are presented together with their interpretation.

[1] J. E. Broadwell and C. N. Tsu, "Transient Pressures Caused by Rocket Start and Shutdown in Ducted Launchers," J. Spacecraft 4 (10), 1323 (1967).

II. THE SILO FLOW

The silo from which the Minuteman missile is fired is a simple straight cylindrical tube as shown in Figure 1(a). When the rocket engine is ignited, the flow and the associated transient pressure wave may be understood by examining the wave diagram of Figure 1(b) for a simple straight tube. The sudden initiation of flow at the bottom of the silo when the rocket motor is ignited can be likened to a piston suddenly put into upward motion at the bottom of the silo. The piston displaces the ambient air, producing compression waves of the "R" family in the ambient air. An equivalent piston velocity $\overline{U}_p$ can be defined that marks the speed of the interface between the driving exhaust gases and the initial ambient air.

At the open end at the top of the silo, the boundary condition of ambient pressure requires that the pressure waves reflect rarefaction waves ("Q" family) of equivalent strength to that of the pressure waves. These resulting waves subsequently reflect from the rigid bottom of the silo as another family of expansion waves (R), which in turn reflect from the free surface at the open end again as compression waves (Q). By this time the wave interactions have increased the local flow velocity until the silo is flowing full of the hot exhaust gas in a quasi-steady state. For typical shallow Minuteman silos, calculations indicate that rocket exhaust would fill the silo in approximately 0.15 sec. This is shown in Figure 1(b) by the path of the interface between the exhaust gases and the air initially in the silo.

The pressure measured by gages at any station a distance x above the silo floor is the sum of these weak acoustic compression and rarefaction waves, which produce a pulse with a compression and a rarefaction phase as shown in Figure 2. The characteristic shape is produced by the phase shifts between the times of arrival of the various families of waves. The magnitude of both compression and rarefaction phases also decreases significantly between the bottom of the silo and the exit. This trend is also

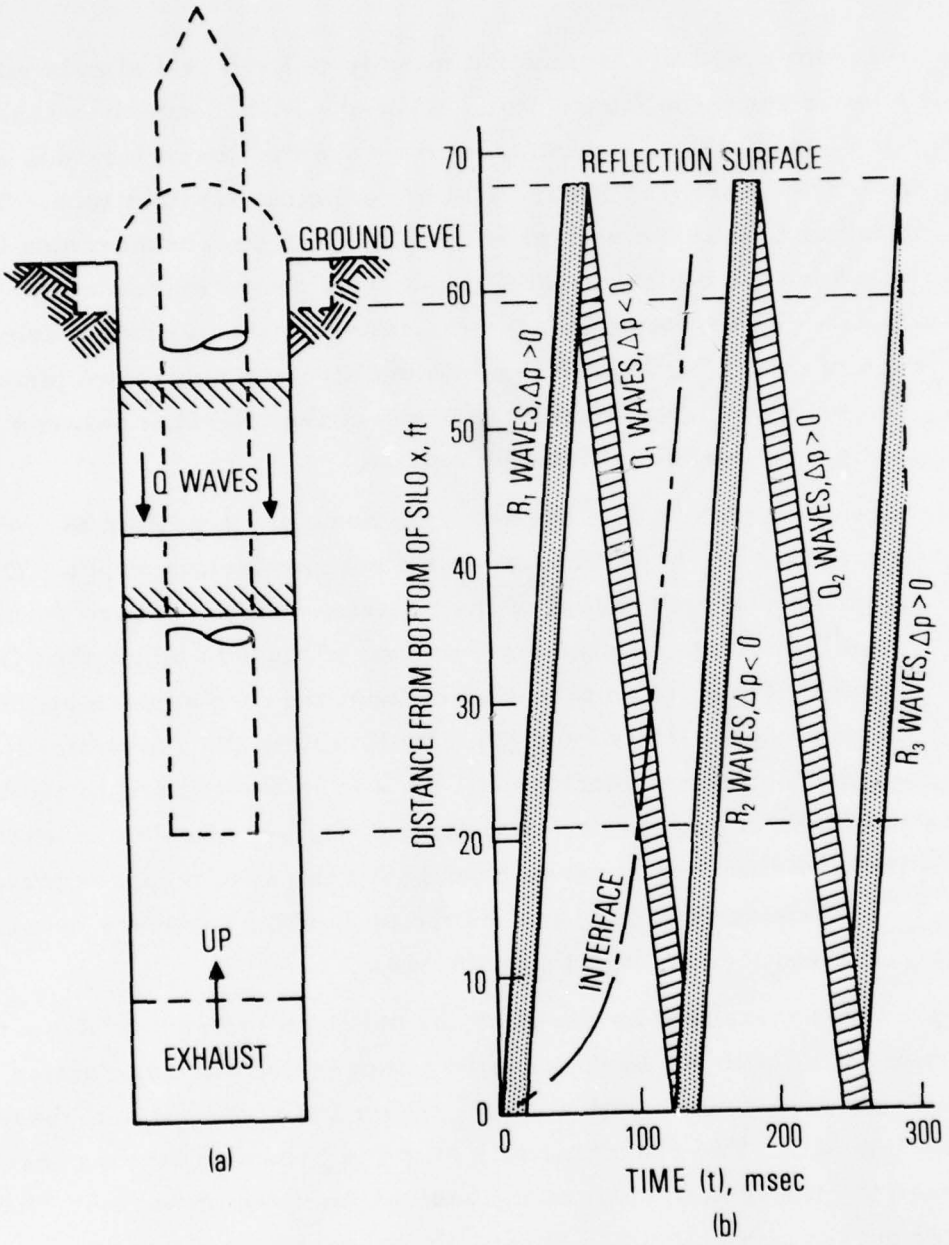

Figure 1. Idealized Missile Launching Silo (a) and Schematic of Wave Diagram in Silo (b)

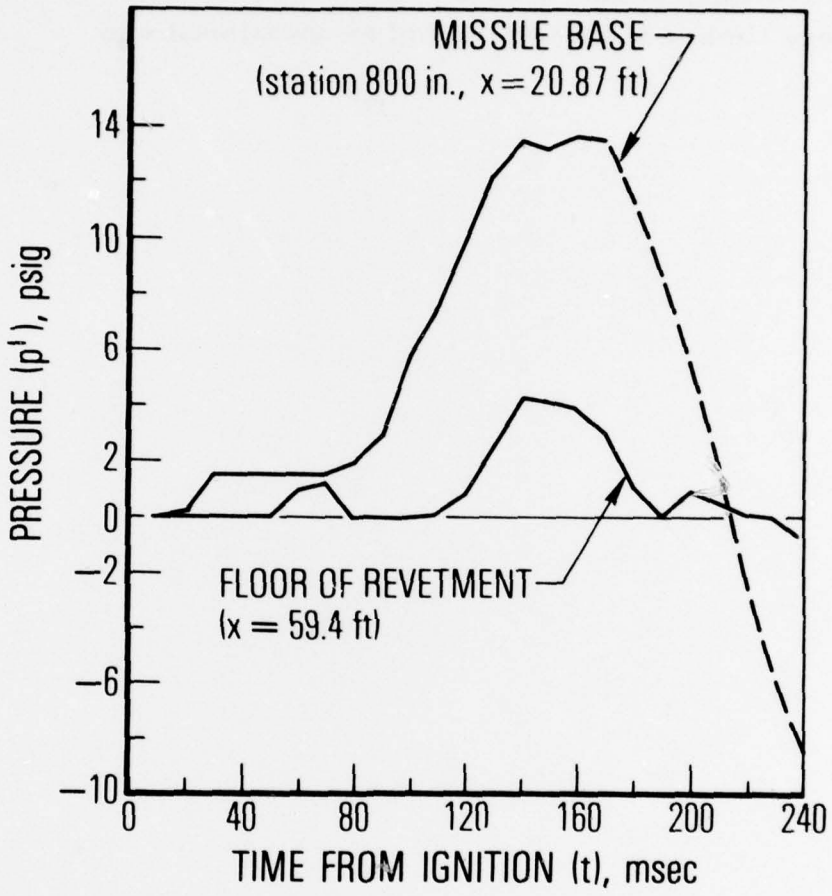

Figure 2. Predicted Pressures at the Base of the Missile and Near the Exit of a Silo

illustrated in Figure 2, which shows the estimates made from the linear acoustic analysis of Broadwell and Tsu,[1] for the pressure histories at the missile base and close to the top of the silo. The predictions for the base region are very similar to observations of an operational silo.

III. THE SHOCK TUBE FLOW

In the shock tube the transient pressure wave, i.e., the shock wave, is produced in the air initially in the driven section as a result of the piston action of the high-pressure gas initially in the driver section. The similarity between the action of the rocket exhaust gas and the driver gas is at once apparent. However, in the shock tube the compression wave generated results from the cumulative effect of the series of acoustic waves generated as the diaphragm breaks. These waves have coalesced to form a shock wave with definite speed and pressure. The shock does reflect at the open end of the tube with 180° phase change. Consequently, it too becomes a rarefaction wave.

An x-t diagram for the shock tube comparable to that of Figure 1(b) for the silo is shown in Figure 3. The incident shock U_s, the advancing contact surface, the rarefaction wave reflected from the open end of the shock tube, and the reflected rarefaction wave from the upstream end of the shock tube driver are all indicated.

In Figure 4 predicted pressure profiles corresponding to the silo profiles of Figure 2 are shown. The principal differences between the silo and shock tube flows are the sharpness of the pressure rise in the shock tube flow, and the absence of decay in peak pressure level for the shock wave as it approaches the open end of the shock tube.

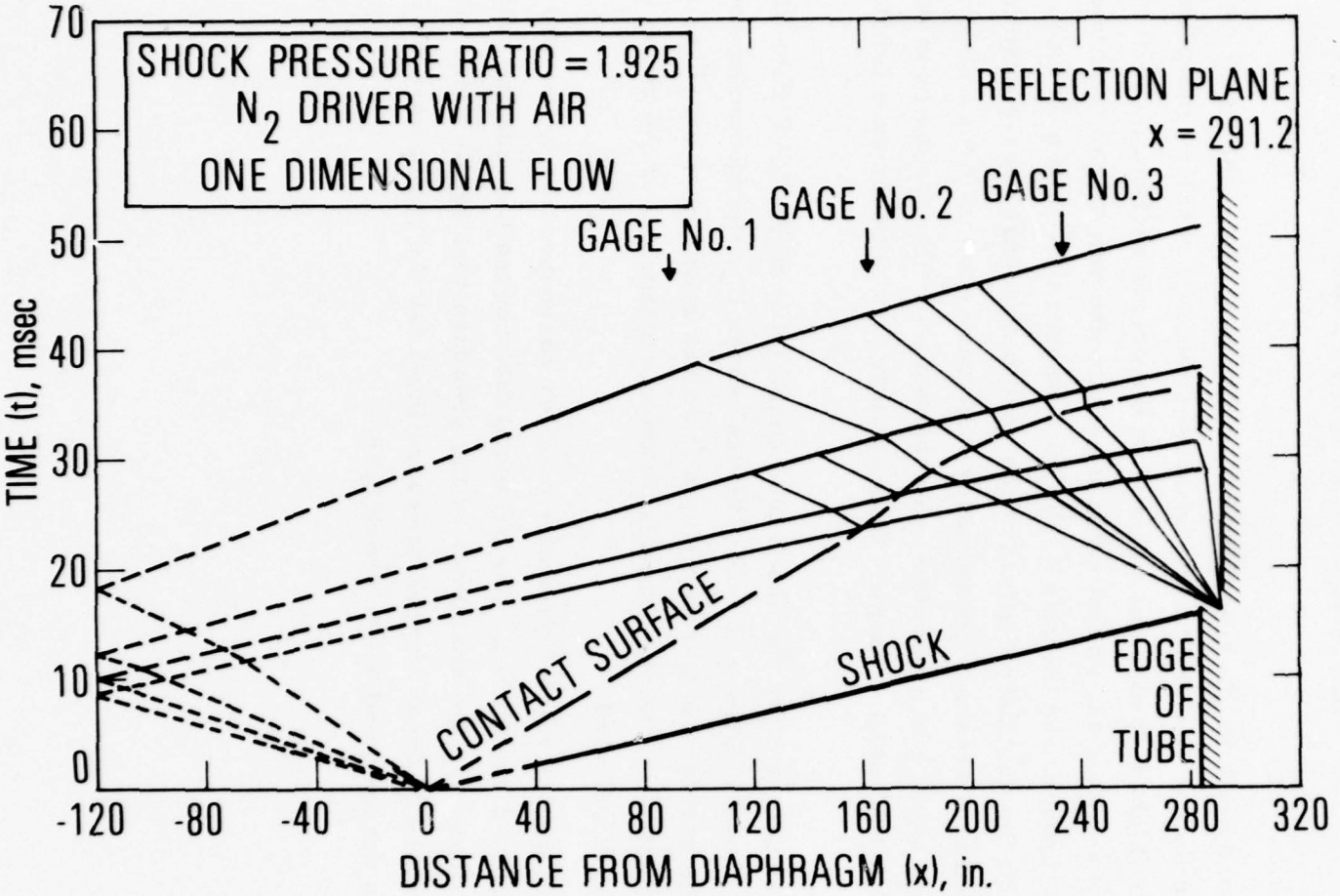

Figure 3. x-t Diagram of Shock Wave, Interface, and Upstream and Downstream Reflected Rarefaction Waves in Open-Ended Shock Tube. $M_s = 1.34$; $p_2/p_1 = 1.95$; $p_1 = 14.7$ psi

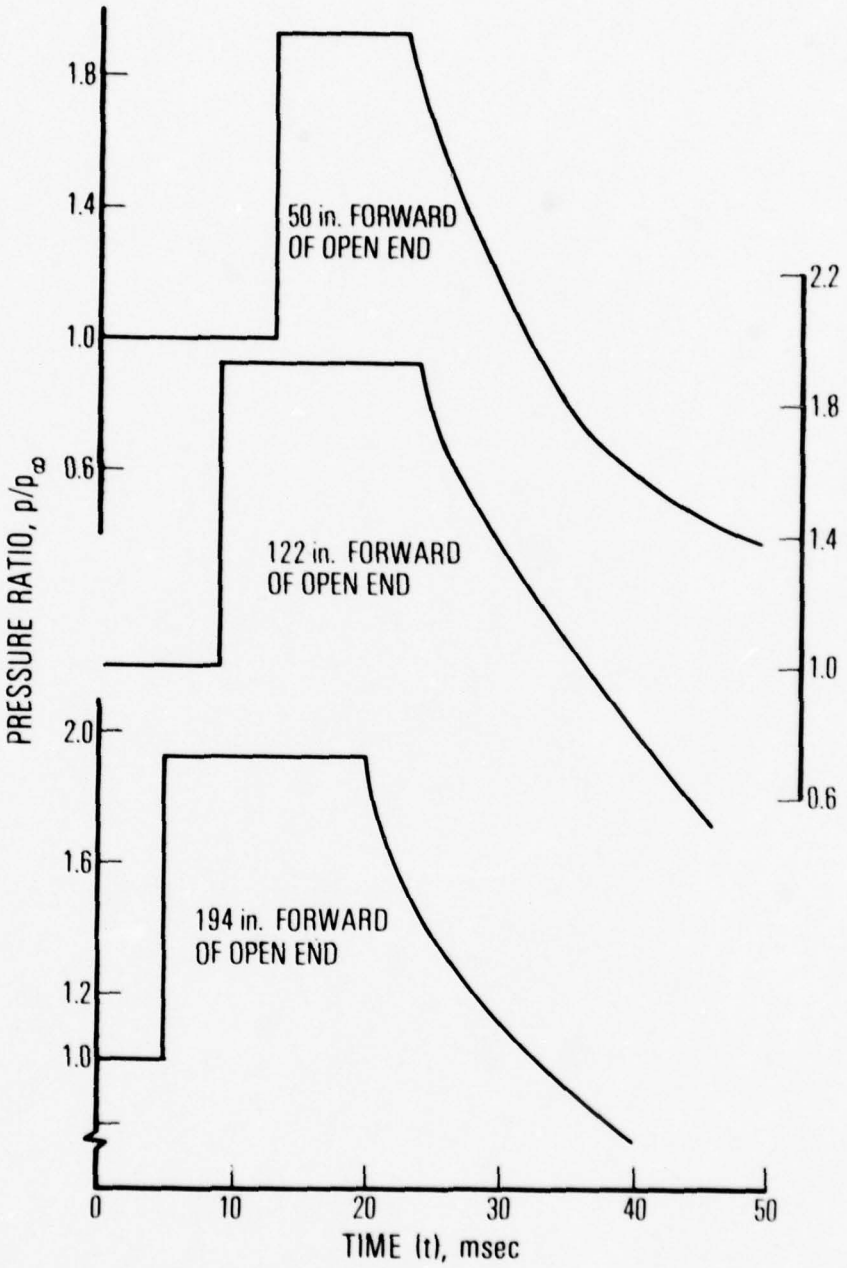

Figure 4. Predicted Pressure Magnitude and Profile in Shock Tube at Various Distances from Open End

IV. EXPERIMENTAL FACILITY

The Aerospace Corporation Low Density Shock Tube was used to simulate the silo. This facility is shown in Figure 5. The driven section that represents the silo has an inside diameter of 17 in. and is about 24 ft long. Since typical Minuteman silos are 12 ft in diameter, this corresponds to an experiment scale of 0.118. The shock tube driver has an inside diameter of 3 in., and a transition section 4 ft long bridges the gap between the driver and larger diameter driven section. High pressure in the driver compensates for the unfavorable driver-to-driven section area ratio so that adequate shock Mach number is obtained.

For this configuration, however, the flow in the shock tube is modified by an upstream facing shock wave standing in the expansion region between driver and driven section as a pressure-matching wave.[2] As a result, the pressure profile obtained at a point corresponding to the missile base for the test conditions at which the shock tube is operated is modified as shown in Figure 6. The uniform pressure regime is reduced to about 4 msec from the 8 msec predicted. Hence, only the positive phase of the silo flow shown in Figure 2 can be simulated.

At the exit of the shock tube the revetment structure characteristic of the silo is reproduced in scale along with a ground plane. A structure simulating the umbilical tower is included in the revetment area. A scale model of the expendable environmental structure is mounted over the end of the silo as shown in Figure 7. The material of the structure is styrofoam, the same fabric from which the full-scale structure was made. All dimensions were scaled according to a one-dimensional analysis, duplicated if time and thickness were similarly scaled.

A large dump tank surrounds the model test field so as to minimize the environmental impact of the shock tube firing. This tank has an inside

[2] David A. Russell, "Orifice Plates in a Shock Tube," Phys. Fluids 5, 4 (1962).

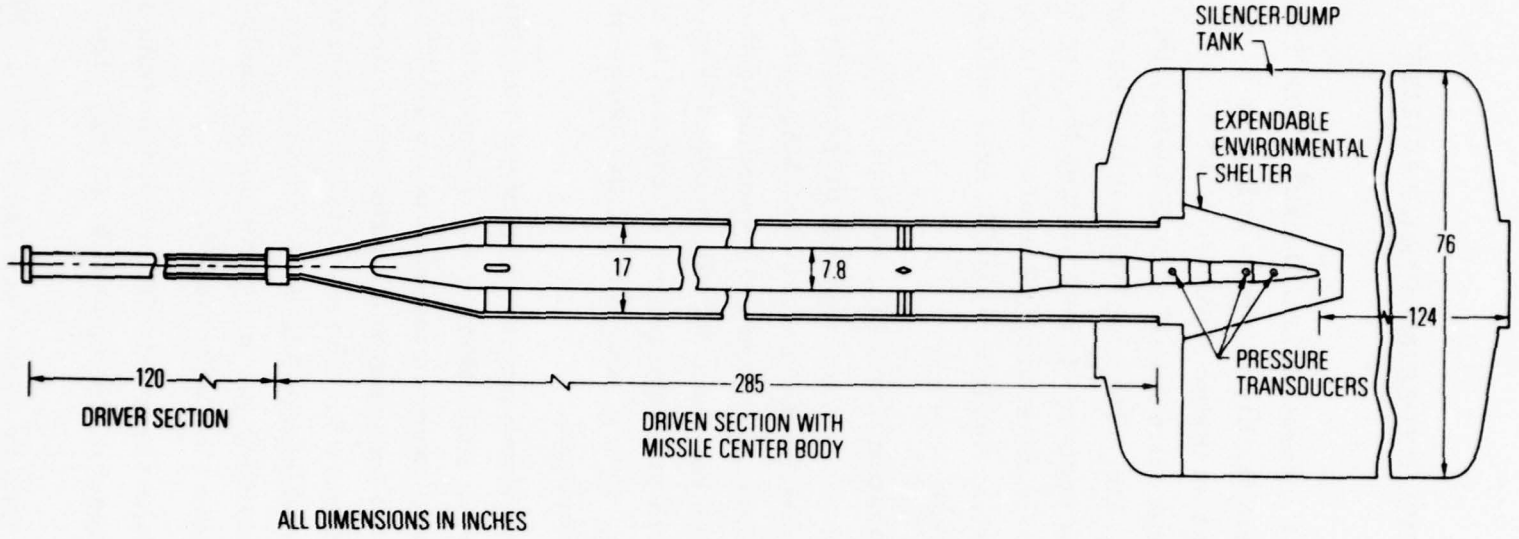

Figure 5. Low Density Shock Tube Modified to Simulate Silo with Minuteman Missile Centerbody

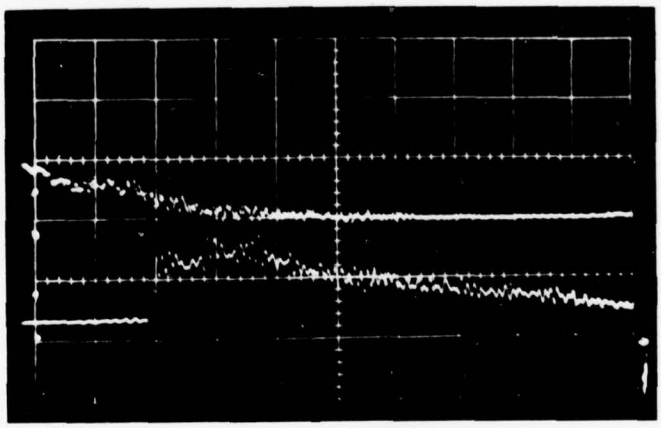

Figure 6. Pressure in Shock Tube 10-1/3 feet Upstream from Shock Tube Exit; Upper Trace is Trigger Gauge Signal; Sweep rate - 2 msec/div; Ordinate - 10 psi/div

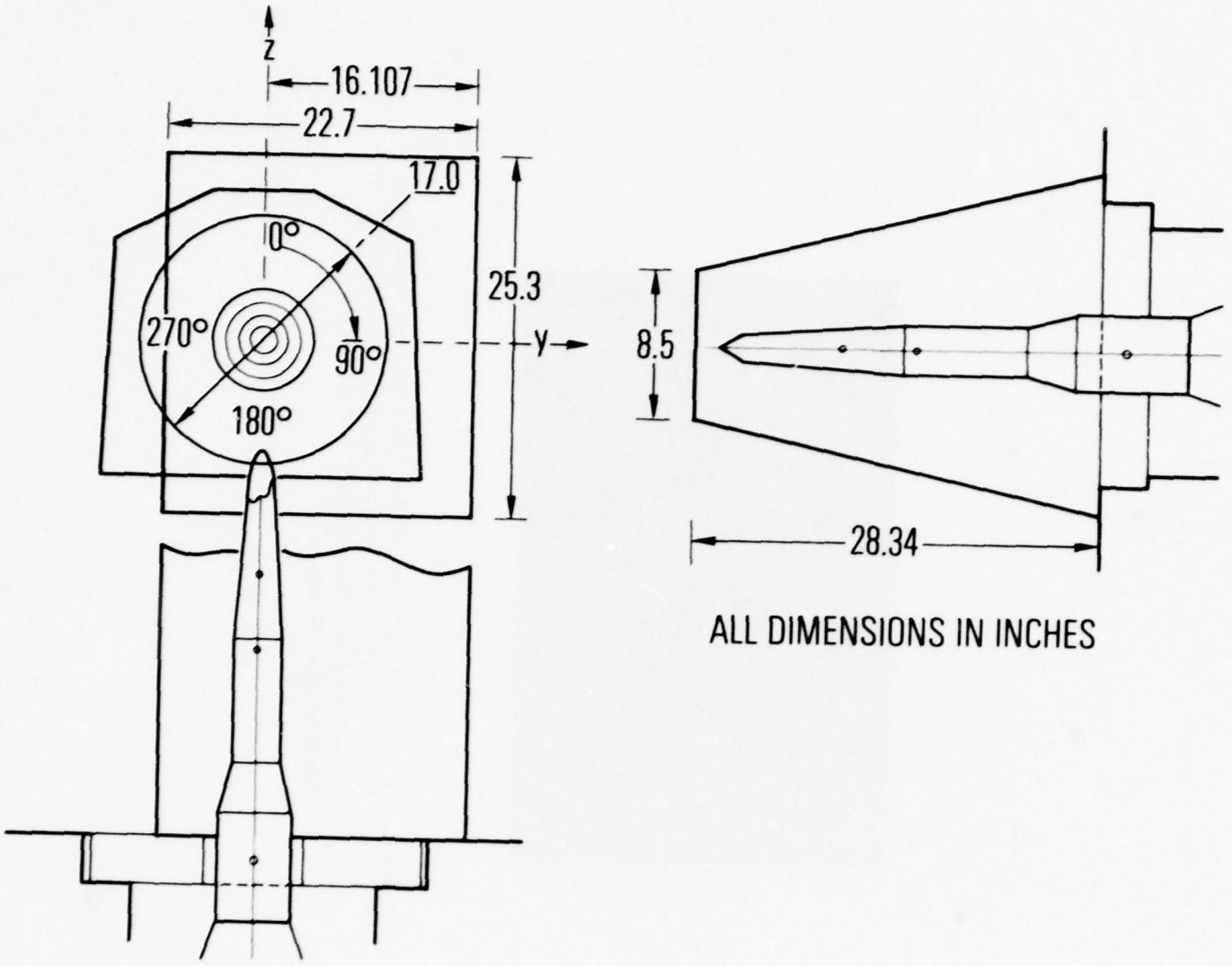

Figure 7. Revetment and Expendable Environmental Shelter Showing Asymmetries Associated with Each. The X direction is along the axis of the vehicle model.

diameter of 76 in., and the end wall is 10-1/3 ft from the tip of the model missile. Therefore, a reflection signal from the side walls of the tank arriving back at the model limits the undisturbed test time to about 6 msec. The shock wave from the end wall takes 20 msec to reach back to the tip of the model.

Twelve pressure transducers (four Atlantic Research Corp. Model LC-60 and eight Endevco Model 8510) were installed on the model as shown in Figure 5, along rays at 0, 90, 180, and 270, at three axial locations 8.5, 13.6, and 27.5 in. from the nose. These gages were expected to sense the surface pressure distribution on the model and hence reflect the change in flow conditions when the exit configuration of the modeled silo was changed.

As previously noted, the scale of the experiment is 0.118. Time is also scaled according to this factor. Pressure is duplicated. Thus, the pressure in the shock tube corresponding to the missile base location in the silo should be on the order of one atmosphere (5 to 15 psi) for about 10 msec. As noted earlier, the pressure (Figure 6) is flat for only about 4 msec, but even after 10 msec it is down by only a half. Since test time in the modeled test site is limited to around 6 msec by the arrival of waves from the walls of the tank surrounding the test area, the pressure profile obtained in the shock tube is not limiting.

V. EXPERIMENTAL RESULTS AND DISCUSSION

The objective of these tests was to determine the effect of the silo exit geometry as it can be modeled in a shock tube. To do this, we examined the pressure distribution on the model for three different silo exit geometries: a completely symmetrical silo to establish a reference, a revetment configuration with asymmetries in the 0 to 180 direction, and a configuration with the expendable environmental structure added. This last configuration had asymmetry in the 90 to 270 direction. These geometries are shown schematically in Figure 7; a photograph of the second one is shown in Figure 8.

Typical pressure measurements for the symmetric configuration, the revetment configuration, and the configuration with the expendable shelter added are shown in Figures 9, 10, and 11.

For the symmetric case, the results can be described referring to Figure 5, considering first that the revetment, ground plane, and expendable shelter are removed. The pressures observed on the model then are the pressures behind an expanding shock wave. Thus, at the shock tube exit the pressure wave still has a flat top for a very short time. Further downstream where expansion has already occurred, the pressures on the centerbody decay rapidly, reflecting the pressure history of the expanding wave. The peak pressure levels fall from about 10 psi close to the tube exit to 3-1/2 and 2-1/2 psi at 14 and 19 inches downstream, respectively.

When the revetment is added (Figure 5), the expanding shock wave reflects from the slightly increased revetment "diameter." This reflected wave is observed on the traces at the shock tube exit and at the downstream positions about 1 msec after the initial shock wave. As the flow expands at the open end of the tube, a negative phase is reflected back up the shock tube. This negative phase is shown on the pressure history observed by the gages at the base of the model upstream of the end of the shock tube.

Figure 8. Minuteman I Model Projecting from Shock Tube with Revetment; Scale = 0.118

RAY, deg	GAGE	CALIBRATION, psi/div
0	p_{31}	6.88
270	p_{34}	9.0
180	p_{33}	7.74
90	p_{32}	7.9
0	p_{21}	2.5
270	p_{24}	2.65
180	p_{23}	2.75
90	p_{22}	3.2
0	p_{11}	2.60
270	p_{14}	2.20
180	p_{13}	2.60
90	P_{12}	2.15

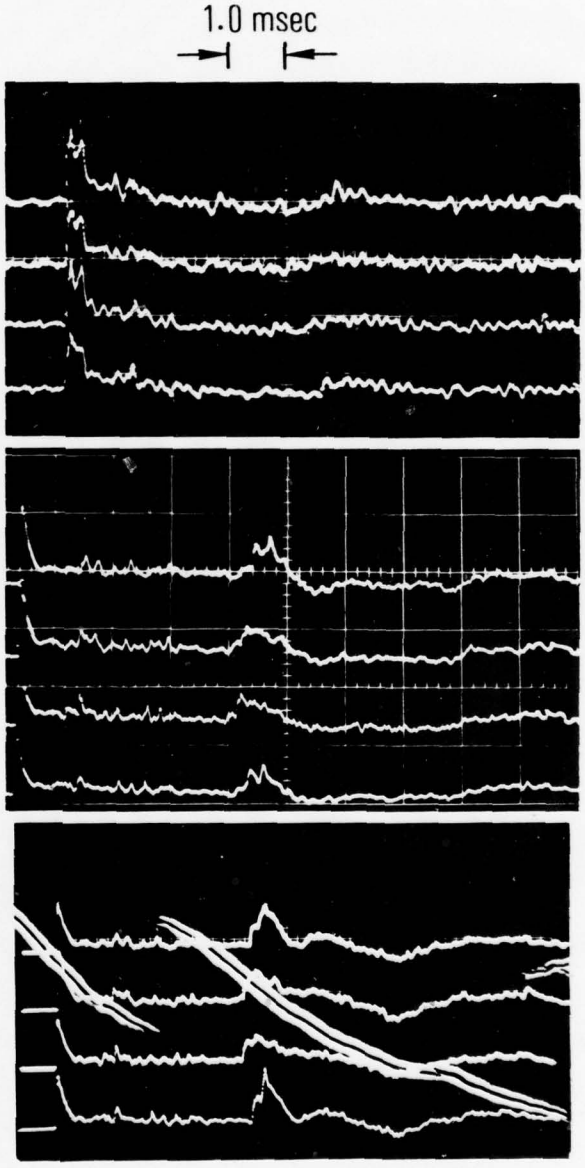

Figure 9. Surface Pressure at Axial Positions 27.5, 13.57, and 8.5 in. from Model Nose at 0, 90, 180, and 270° Rays; Symmetric Configuration

RAY, deg	GAGE	CALIBRATION, psi/div
0	p_{31}	6.88
270	p_{34}	9.0
180	p_{33}	7.74
90	p_{32}	7.9
0	p_{21}	2.5
270	p_{24}	2.65
180	p_{23}	2.75
90	p_{22}	3.2
0	p_{11}	2.60
270	p_{14}	2.20
180	p_{13}	2.60
90	p_{12}	2.15

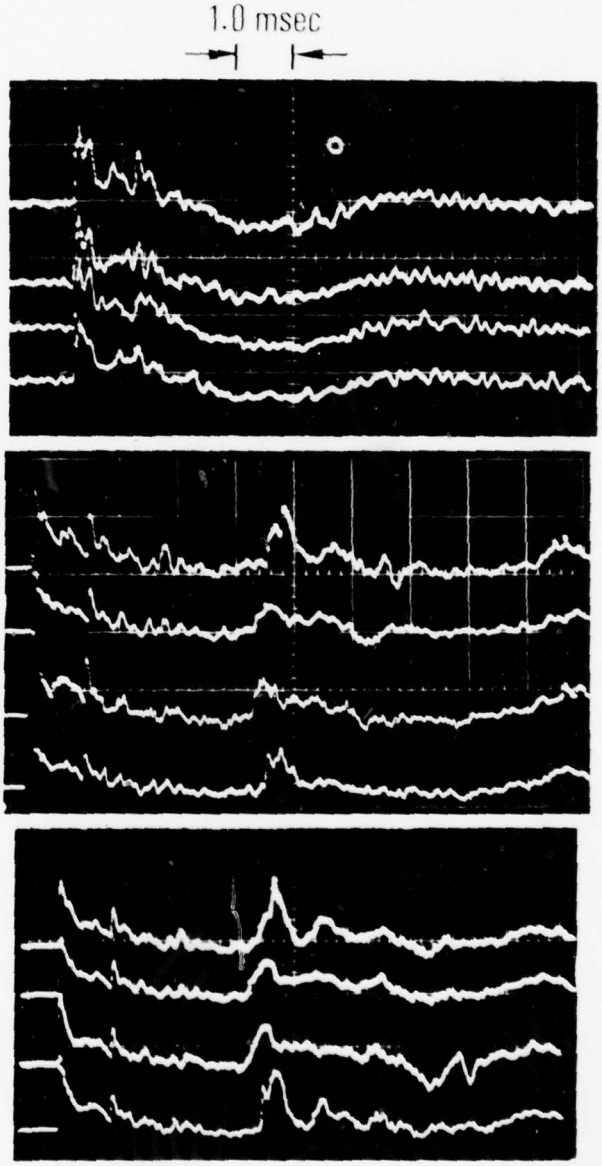

Figure 10. Surface Pressure at Axial Positions 27.5, 13.57, and 8.5 in. from Model Nose at 0, 90, 180, and 270° Rays; Revetment Configuration

RAY, deg	GAGE	CALIBRATION, psi/div
0	p_{31}	6.88
270	p_{34}	9.0
180	p_{33}	7.74
90	p_{32}	7.9
0	p_{21}	2.5
270	p_{24}	2.65
180	p_{23}	2.75
90	p_{22}	3.2
0	p_{11}	2.60
270	p_{14}	2.20
180	p_{13}	2.60
90	p_{12}	2.15

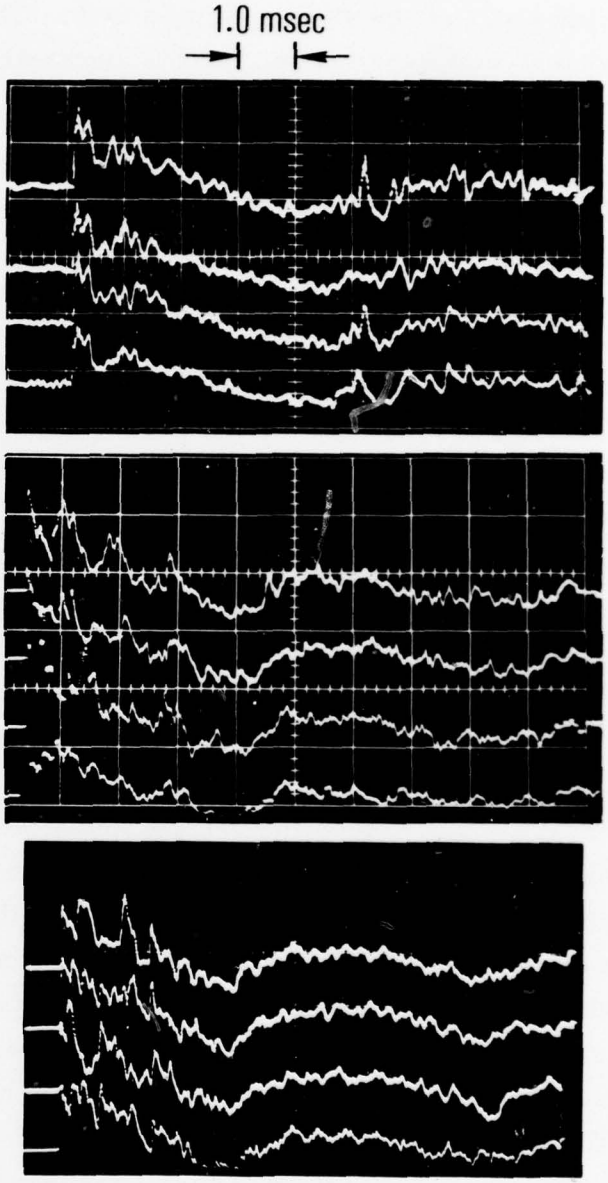

Figure 11. Surface Pressure at Axial Positions 27.5, 13.57, and 8.5 in. from Model Nose at 0, 90, 180, and 270° Rays; Expendable Foam Shelter Added

About 4 msec after the shock passes the two downstream gage stations, a pressure pulse is observed. This wave is the acoustic wave reflected from the side walls of the silencer-dump tank. This wave limits the test time of interest to just over 4 msec for the symmetric and revetment configurations.

The measurements shown in Figures 9, 10, and 11 have also been recorded on magnetic tape. As a result, these data can be manipulated automatically by means of computer to obtain pressure differences between opposing gages at the three axial stations. The sampling rate and filtering of the data were chosen to be commensurate with the gage installation frequency response, which was about 6 kHz minimum. For the symmetric configurations, these pressure differences along the y and z directions at the 27.5 in. station are shown in Figure 12; for the revetment configuration, they are shown in Figure 13. Although there is much fluctuation in the pressure differences, there appears to be little net trend in pressure loading in either the y or z direction for the symmetric configuration. However, for the revetment configuration a significant net side pressure appears for the z direction. The load peaks during the negative phase of the pressure traces shown in the top oscilloscope records of Figure 10. For the earlier axial stations the pressures are smaller as indicated; the pressure differences are accordingly also smaller. They further show no net trend in side loading. Only the gages at the most aft position on the vehicle model seem to have significant net side pressure. Thus, several differences appear in the pressure measurements which may be attributed to the presence of the revetment. First, the shock tube length is extended, thus locating station 27.5 gages inside the end of the shock tube. Therefore, the reflected rarefaction wave moving upstream in the shock tube is observed as a negative pressure. In addition, shock waves reflected from the expanded extension also are detected at this gage station. Lastly, a net pressure is noted at this station in the z direction, which, significantly, is the direction of the asymmetry of the revetment.

When the expendable shelter is installed, the pressure measurements are substantially changed at the two stations close to the model nose. The

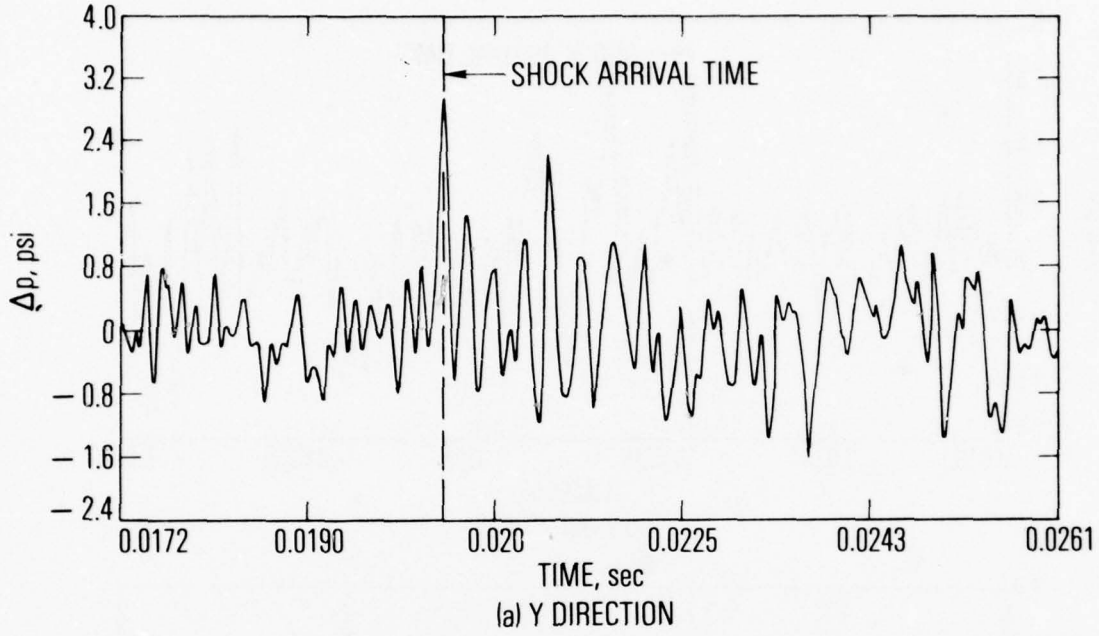

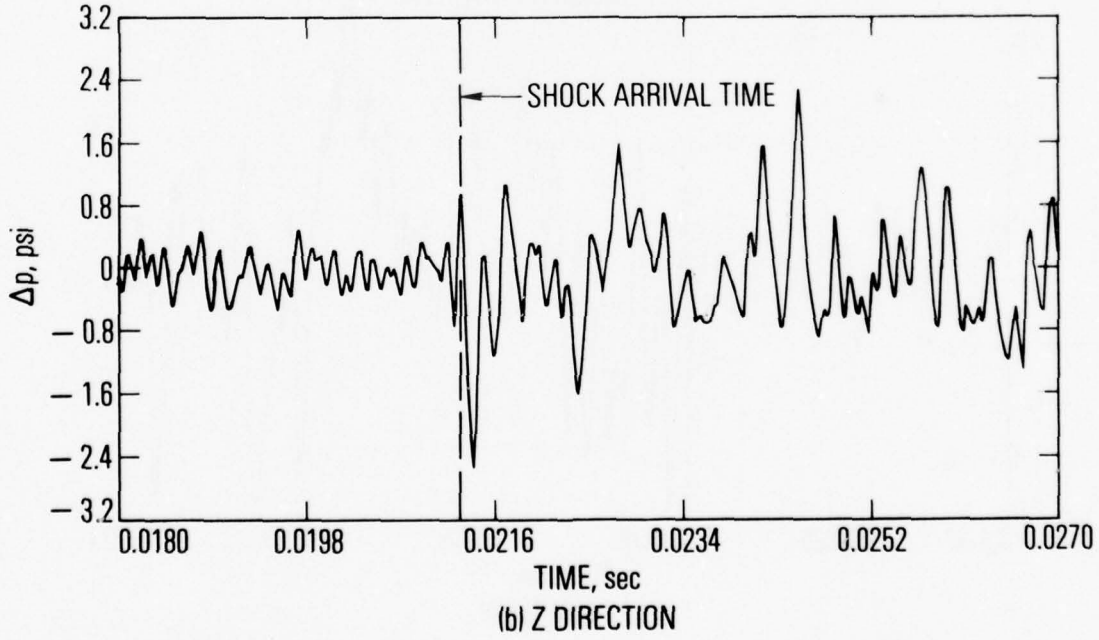

Figure 12. Pressure Difference at Station 27.5 for Symmetric Configuration

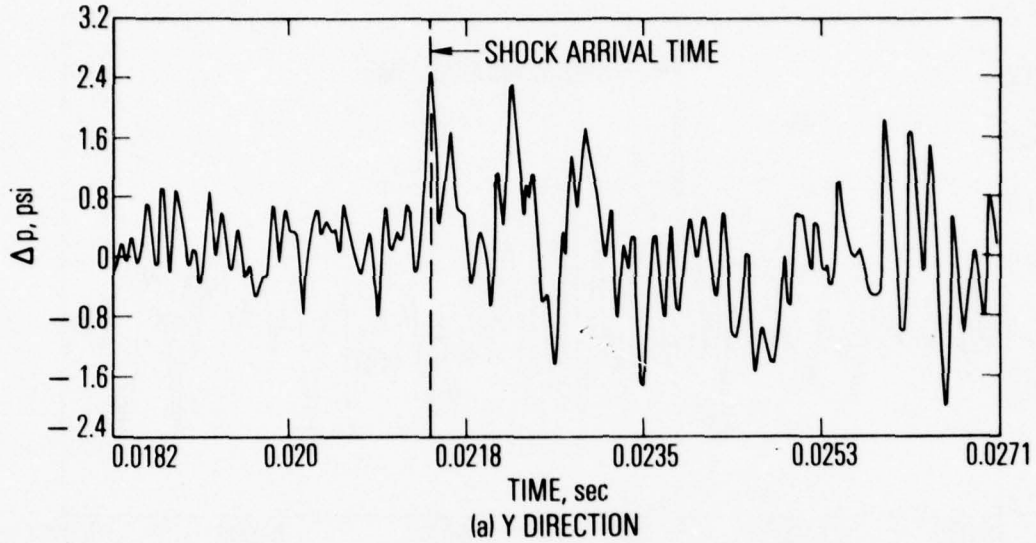

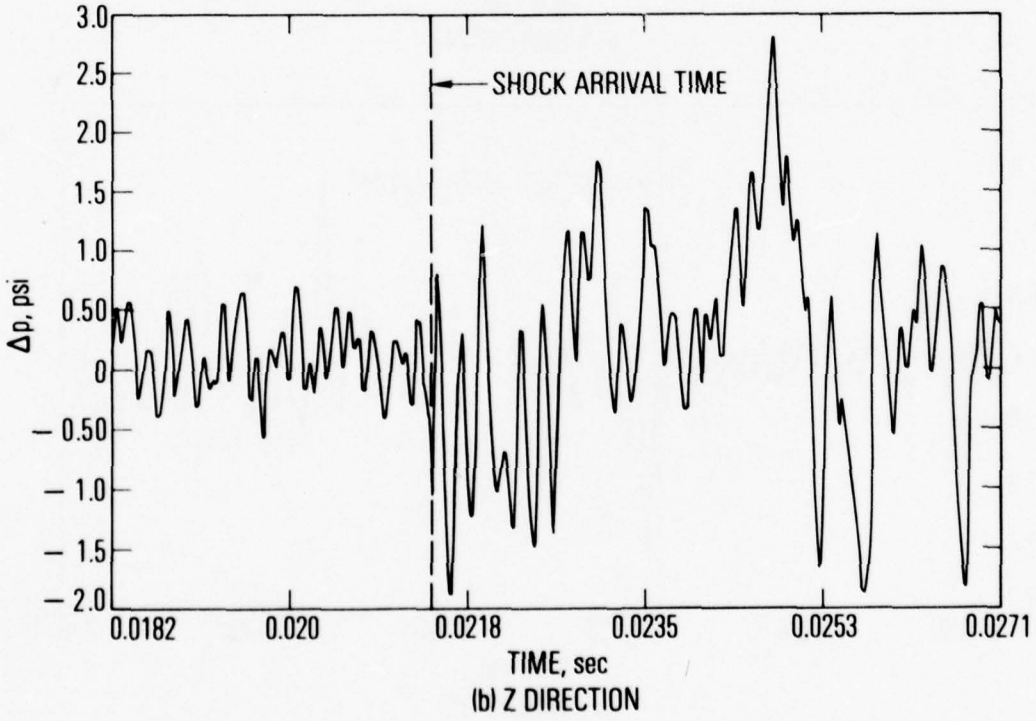

Figure 13. Pressure Difference at Station 27.5 for Revetment Configuration

shocked gas flowing from the tube is reflected from the walls of the shelter, and the arrival of these reflected waves at the missile model surface is indicated by sharp rises on the pressure history. For the position closest to the nose, reflections appear to take place. Then, as the shelter begins to disintegrate and drift away, about 1-1/2 msec after the initial pressure arrives, the pressure at these stations drops below ambient pressure. High-speed motion pictures of the shelter breakup were made. These were time-correlated to the pressure measurements so that the time when the shelter began to move was determined relative to the pressure histories.

Pressure differences between opposing pressure gages at the three axial stations were also determined for the shelter configuration. From these data, shown in Figures 14, 15, and 16, it is seen that at the forward gage positions there is little net asymmetry in the pressure differences in the z direction. This is to be expected since the shelter is symmetric with respect to the vehicle model in the plane of this direction. A net load does seem to appear in the y direction at all axial stations, reflecting fairly well the closeness of one wall of the shelter.

In an effort to gain greater insight into the pressure-force time-history, and possibly into the physical mechanisms which determine that history, a computer program was developed to transform the 0 to 180° and 90 to 270° orthogonal rectangular coordinate pressure-difference signals into a polar coordinate (or vector magnitude, vector direction) representation of the signature. Attention was focused upon the ring of four pressure transducers at station 27.5, where (at least with the revetment in place) the effect of the reflected waves from the sidewalls of the dump tank seem to be minimized, and the absolute magnitudes of the pressures and the pressure difference forces are relatively large. This work is discussed in detail within Appendix A. In brief, the vector magnitudes for the revetment and revetment plus SES cases were both significantly larger than that for the symmetric case. Similarly, for direction, the

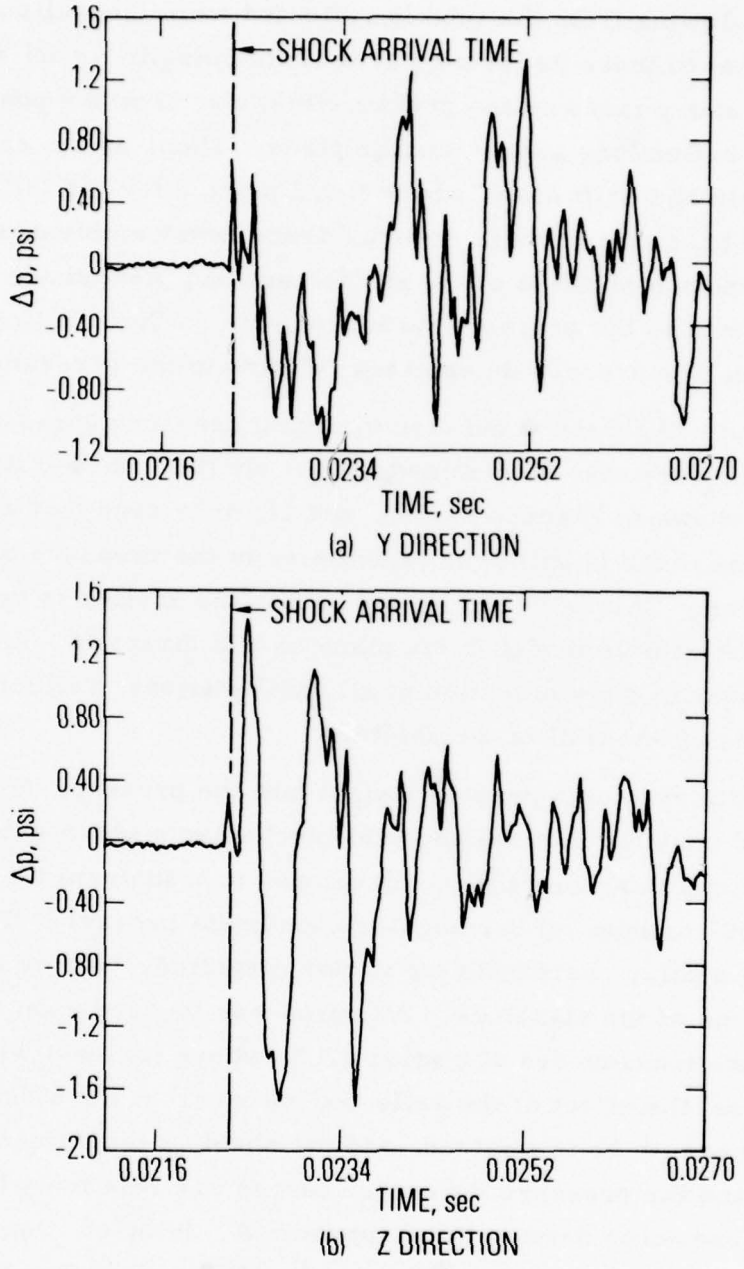

Figure 14. Pressure Difference at Station 8.5 for Shelter Configuration

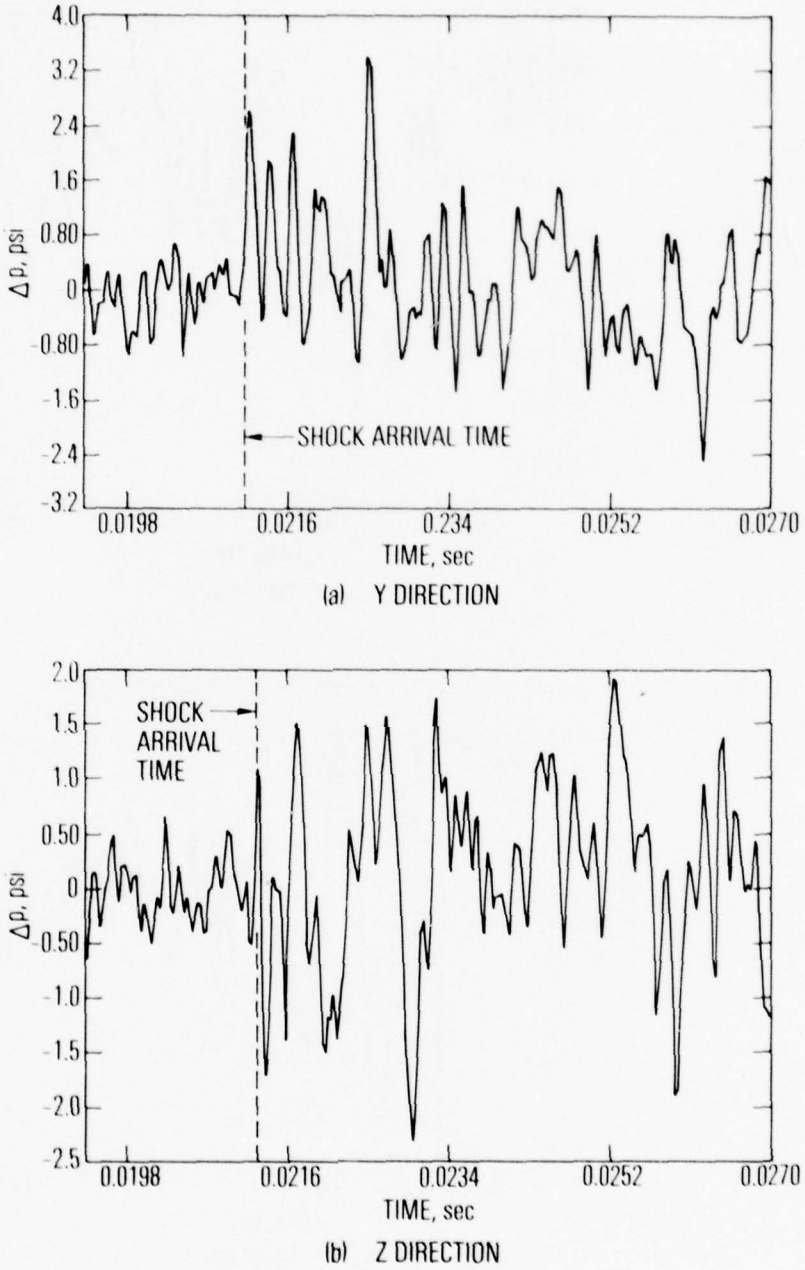

Figure 15. Pressure Different at Station 13.57 for Shelter Configuration

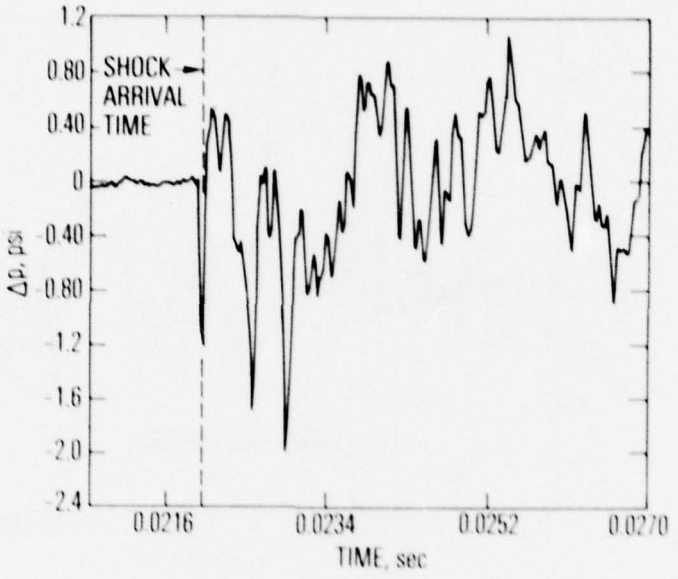

(a) Y DIRECTION

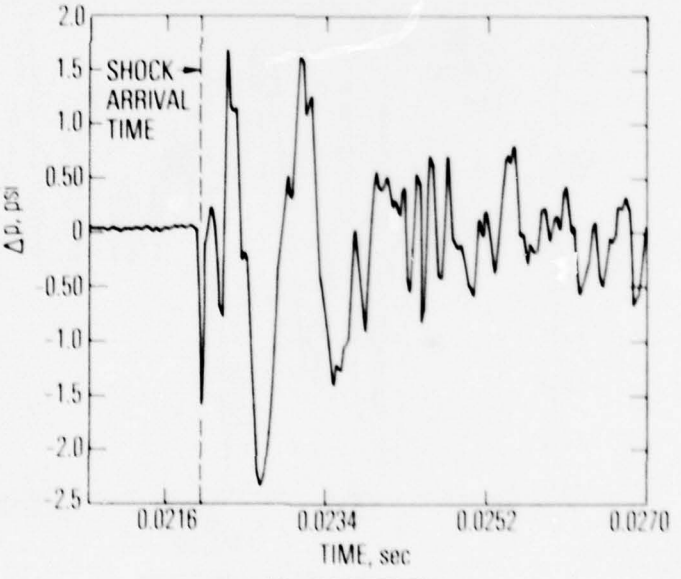

(b) Z DIRECTION

Figure 16. Pressure Difference at Station 27.5 for Shelter Configuration

symmetric case showed relatively limited swings in direction compared with the revetment and revetment plus SES cases. In the case of the revetment plus SES, the swings in direction were commensurate with the asymmetry of the SES installation on the silo.

VI. APPLICATION TO FLIGHT DATA

In Appendix B, the rectangular coordinate to polar coordinate transformation for the time histories, developed for the shock tunnel data, is applied to the flight test data for the November 1977 TDV-3 launch. That launch, conducted subsequent to the present shock tube study, was the first in which a ring of four pressure transducers was mounted in the upper vehicle RAW section. The coordinate transformation was applied to the outputs from those pressure transducers and the nearby two-axis radial accelerometers. The vector magnitude and vector direction resultants for the pressure-difference-force (input) and acceleration (response) are compared. The close correspondence of the input and response directional signatures gives strong experimental confirmation of the hypothesis that the upper vehicle asymmetric pressure force is the principal contributor to the observed upper vehicle response, at least for those vehicles having dynamic characteristics similar to the TDV series. A description of the details of the application of the transformation to the TDV data, a presentation of the time-history comparison, and some remarks on the polar coordinate characteristics for both the full-scale flight data and the laboratory shock-tube results are contained in Appendix B.

VII. CONCLUSIONS

With regard to the effect of varying the shock tube-silo termination, it is concluded that:

a. The presence of the asymmetric revetment affects the pressure loading on the vehicle. The gages on the model in the revetment location show an asymmetric distribution of pressure, which is in the direction of the geometric asymmetry of the revetment.

b. Adding the shelter causes reflected shock waves to impinge on the centerbody-vehicle, and a small net asymmetric loading appears in the y direction, the asymmetric direction of the shelter-vehicle configuration.

c. A data reduction technique has been developed to treat the measurements from the shock tube experiments in which the time varying orthogonal pressure coordinates are transformed into an r-θ coordinate system.

In extending such conclusions to the actual silo-vehicle flows, one must keep in mind the differences in the two flows; e.g., the pressure in the silo flow reflects the slow pressure rise of combustion in the rocket motor relative to the steep-fronted shock wave pressure in the shock tube. Nevertheless, the data reduction technology developed for these shock tube experiments has in fact been applied to treat full-scale launch vehicle surface pressure measurements and vehicle accelerometer measurements. This treatment showed a strong correlation between these two quantities for the TDV-3 launch. Thus the conclusion that the accelerations are due to surface pressures originating from the silo exit geometric asymmetries is indicated. Similar, but not indentical, features of the pressure difference force history were observed for vehicle and model during the (scaled) time period in the neighborhood of "lift off" time.

APPENDIX A

PRESSURE FORCE VECTOR RECTANGULAR TO POLAR COORDINATE TRANSFORMATION

A decision was made to perform additional data processing of the output from the four station 27.5 (inside the revetment) pressure transducers, and to look for additional clues to revetment and SES-induced asymmetries from these results. This decision was motivated by several factors: the complex, unsteady three-dimensional flow resulting from the simulated launch made it attractive to concentrate on the conditions at a single axial station and to try to determine the localized directional effects; the station 3 transducers were most protected from the effects of the reflected wave from the dump-tank walls; the largest measured overpressures and largest unit-length projected area exist for station 27.5; and the pressure-time history with the noticeable underpressure period had the closest approach to upper-vehicle histories measured to date.

This appendix presents the results of transforming the 0 to 180° and 90 to 270° orthogonal Δp histories into an r-θ coordinate system, thus obtaining the total Δp vector magnitude and vector direction history at station 3.

DATA REDUCTION PROCEDURE

The electrical representations of the pressure-time histories from the four pressure transducers at station 27.5 are stored on magnetic tape. Upon playback, these signals were lowpass filtered, sampled, digitized, and stored on digital tape after being passed through a calibration program. Additional digital filtering was necessary to remove a presumed acceleration sensitive signal present on the data channels, evidenced by the transition from a state of unnoticeable fluctuation before a time representative of

diaphragm breaking through a period of gradually increasing buildingup of low level random fluctuations before the arrival of the starting shock at the transducer. A special power = 2, 20 half-weights digital filter (minimizing time-domain distortion) was used, and the filter cutoff frequency was altered to give a balance between eliminating the unwanted high frequency mechanical signals and retaining enough of the high frequency character of the pressure signal. A filter cutoff frequency of 2000 Hz was finally selected (which corresponds to a full scale value of 200 Hz).

Diametrically opposed pairs of signals were differenced to obtain the orthogonal pair of Δp traces, oriented in silo coordinates, see Figure 7.

$$\Delta p_{0\text{-}180}(t) = p_0(t) - p_{180}(t) = p_{31}(t) - p_{33}(t)$$

$$\Delta p_{90\text{-}270}(t) = p_{90}(t) - p_{270}(t) = p_{32}(t) - p_{34}(t)$$

These orthogonal Δp histories were then transformed into polar coordinates:

$$r(t) = |\Delta p(t)| = \left\{[\Delta p_{0\text{-}180}(t)]^2 + [\Delta p_{90\text{-}270}]^2\right\}^{1/2}$$

$$\theta(t) = \tan^{-1}\left[\frac{\Delta p_{90\text{-}270}(t)}{\Delta p_{0\text{-}180}(t)}\right]$$

Here, $r(t)$ represents the vector resultant magnitude of the differential pressure forces (per unit area) acting on the vehicle. $\theta(t)$ is the vector resultant angle of this force related to the coordinate system shown in Figure 7 of the main report.

Because of the high frequency fluctuations appearing in the $\theta(t)$ plot at 2000-Hz filter cutoff frequency, alternate lower frequencies were tried to bring out the main trends of this data. A frequency of 250 Hz was selected as being the most effective compromise for final digital filtering of the $\theta(t)$ values.

RESULTS

Six cases were selected for the aforementioned data analysis: two each for the three configurations – symmetrical silo, revetment, and revetment plus SES. Two shots for each configuration were chosen as a compromise between obtaining some measure of the reproducibility of the experiment for the output parameters chosen and expending undue effort and expense in reducing a larger number of cases. Generally good agreement in $r(t)$ and $\theta(t)$ for the two cases for each configuration was found, but there was some variation in magnitude over the ensemble of tests.

Figure A-1 presents the pressure-time history for station 27.5 (0°) with symmetrical silo configuration. This transducer is selected as a typical representative of the four at station 27.5, and the variations between the four stations responsible for $\Delta p(t)$ do not change the overall appearance of these curves vis-a-vis the other positions. The ordinate is in pounds per square inch, which scales one-to-one with full scale pressures. The abscissa is in seconds for the model case; a comparable full-scale case comparison is obtained by multiplying the times by about ten, or exactly 8.5 (the linear model scale). The steep, short starting pulse from the shock tube is noted, and, of course, differs from the slower buildup in the full scale case wherein the pressure wave pattern generated by the relatively slow buildup history of the motor chamber pressure is the generating source. The relatively low magnitude of underpressure for this case is noted. The 2 psi increase after about 0.005 sec from the starting wave may be due to the reflected wave pattern emanating from the dump tank walls. Thus, the primary value of this simulation is during the first 5 msec.

Figures A-2 and A-3 show similar plots for the same position for the cases with revetment and revetment plus SES added. The larger magnitude of the underpressure is noted. The presence of the revetment now partially shields the pressure transducers, and the arrival time and strength of any dump-tank-wall generated reflected waves is not easily deduced.

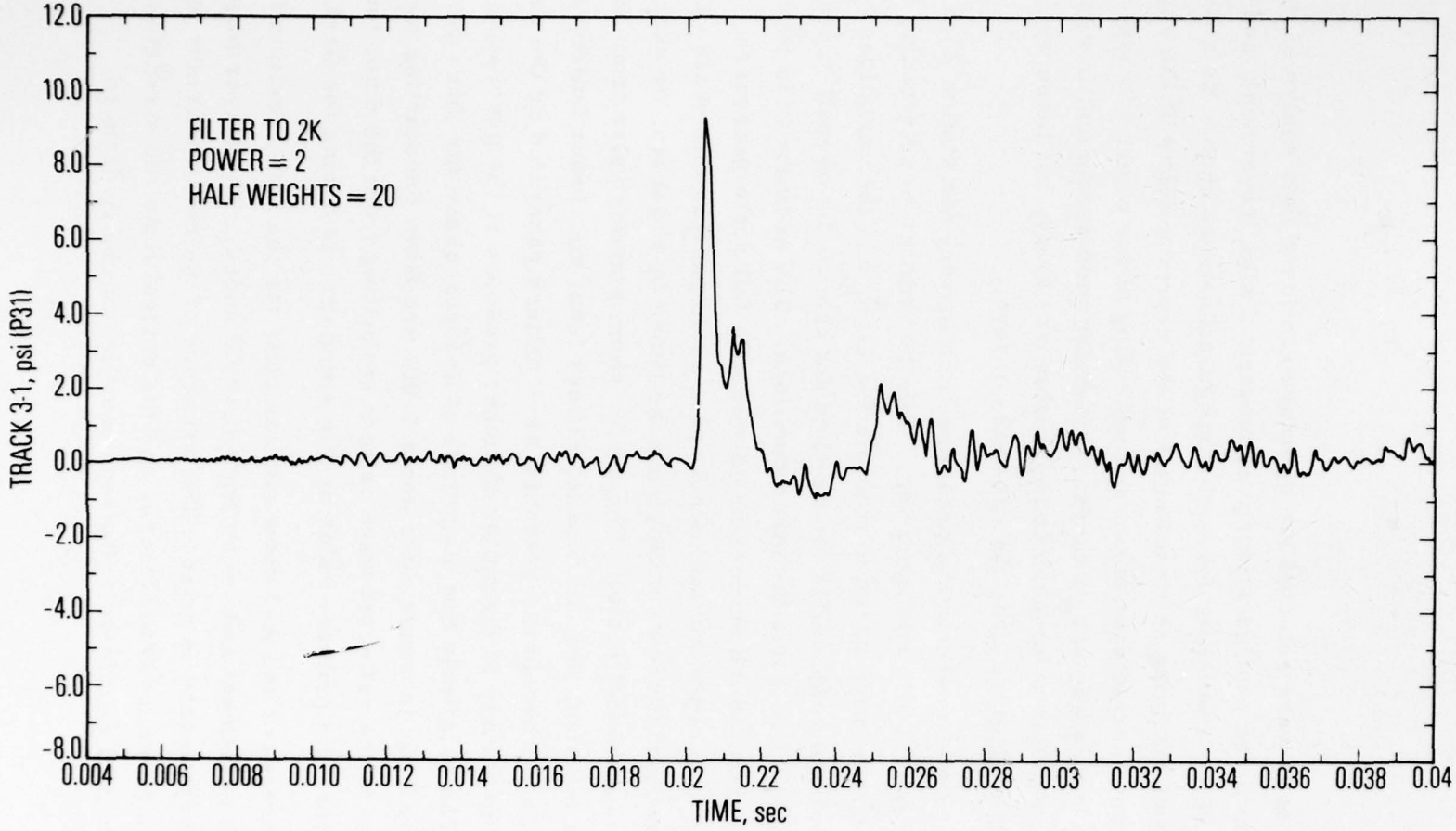

Figure A-1. Symmetrical

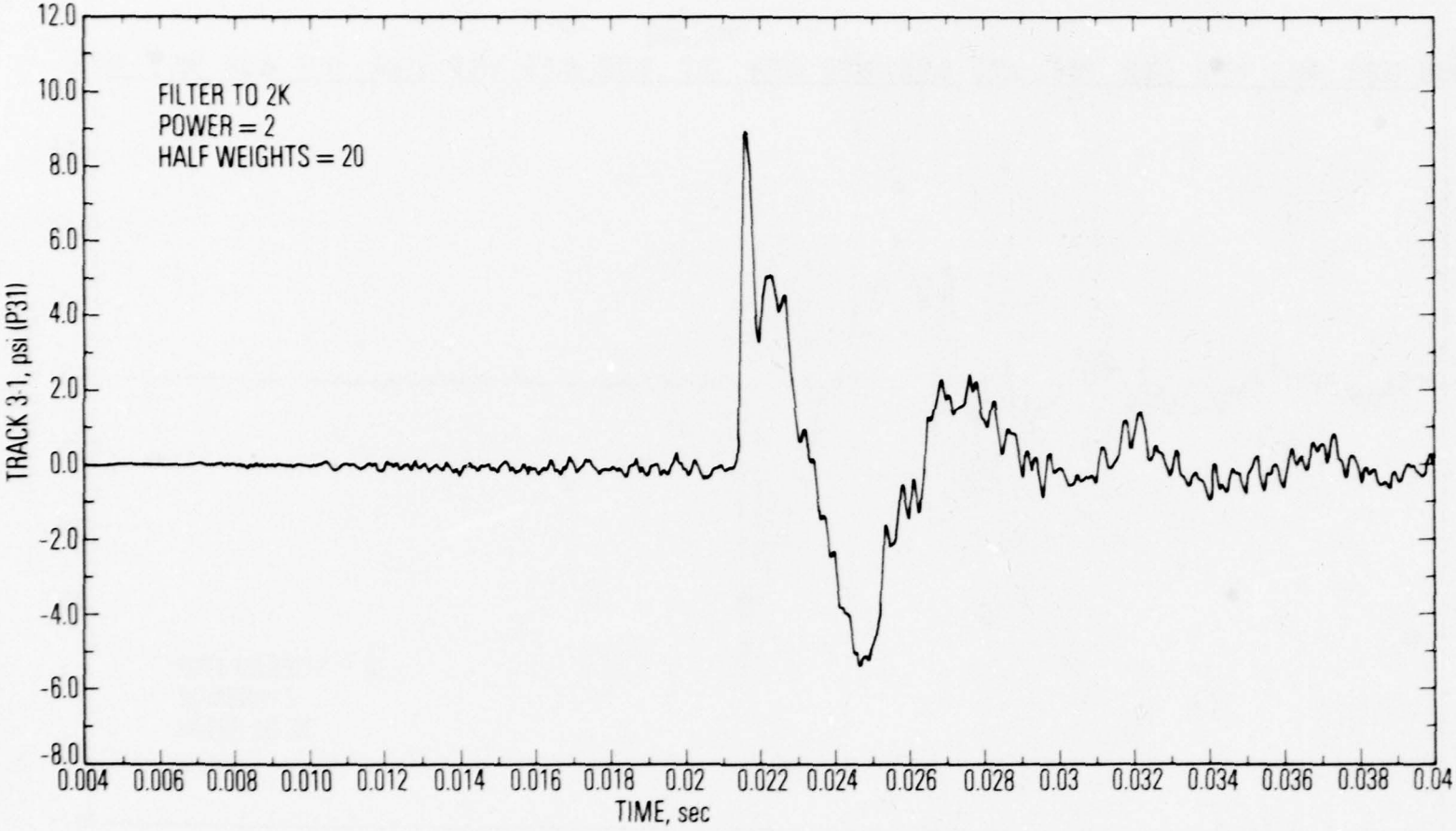

Figure A-2. Revetment

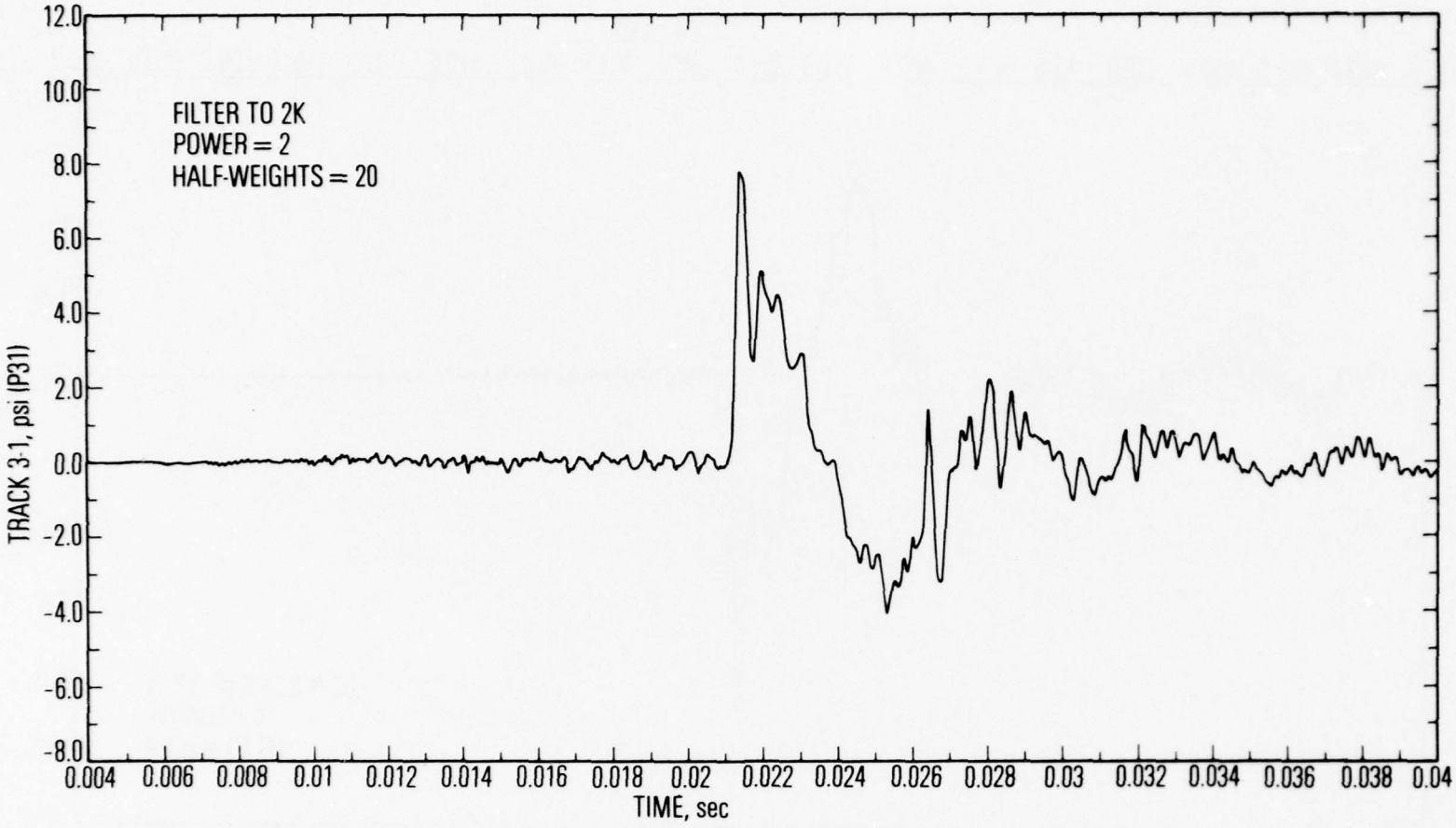

Figure A-3. Reventment + SES

The time origin for Figures A-4 and A-5 was obtained by examination of the first three figures. The peak-pressure time for the starting pressure pulse was taken as $t = 0$ for each of the three representative cases.

Figure A-4 shows the pressure magnitude histories for each of the configurations. The dashed line at $p = 0.4$ psi is taken to be the average of the rms acceleration-dependent signal, determined from the level observed just before $t = 0$. Since the latter level of output signal is assumed to be present even if $\Delta p = 0$ at some particular time, it is suggested that the dashed line should be considered to be a "virtual zero axis" for the evaluation of pressure magnitude. The levels for the symmetrical silo case are well below those for the other two configurations. The levels for the SES added case appear higher than those for the revetment alone, but this evaluation depends to some extent on whether the large amplitude peak at $t = 0.006$ is a consequence of the SES or represents the arrival of a wall reflection. The times designated t_t and t_L, superimposed upon the curves, represent the times that the pressure crosses the zero axis in the downward direction (t_t) and the time for the lowest pressure (underpressure) in the case of t_L. These times are obtained from Figures A-1 through A-3.

Similarly $t = 0$ referenced plots for $\theta(t)$ are shown in Figure A-5. The three cases are plotted on the same axis for comparison. The symmetrical case shows relatively limited and irregular (30° or less) swings around the 180° position; on the other hand, the revetment and then SES cases show increasingly large deviations during the first 5 or 6 msec. The SES case first has a moderate 40° swing above 180° and then executes an almost sinusoidal swing with peaks at 90 and 270°, which represent the positions on the axis of greatest SES asymmetry (offset). This result is consistent with a pressure wave reflection pattern generated by the vertical, offset, SES walls. The angular variation as a function of time corresponds to about a 60-Hz rotation of the pressure force around the vehicle axis for the full-scale case.

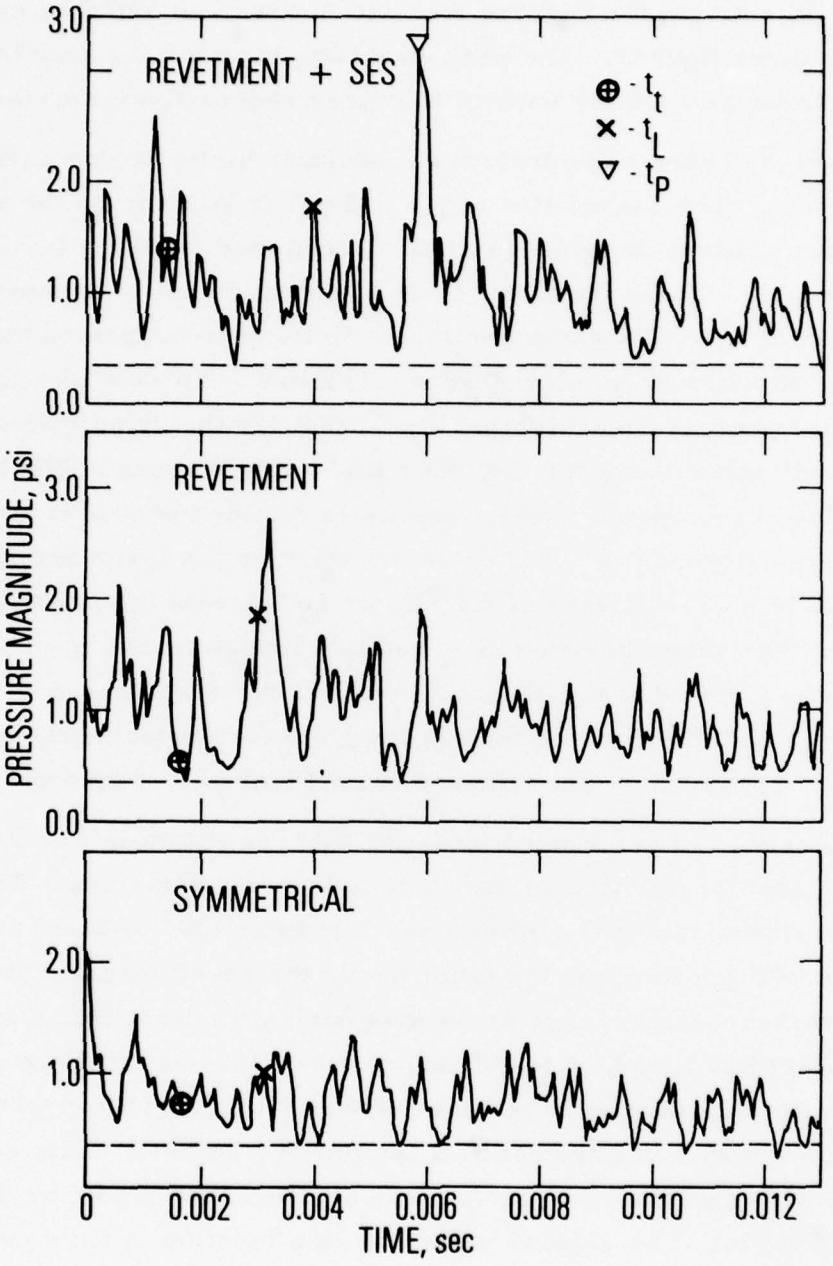

Figure A-4. Time History of Pressure Differential Magnitude

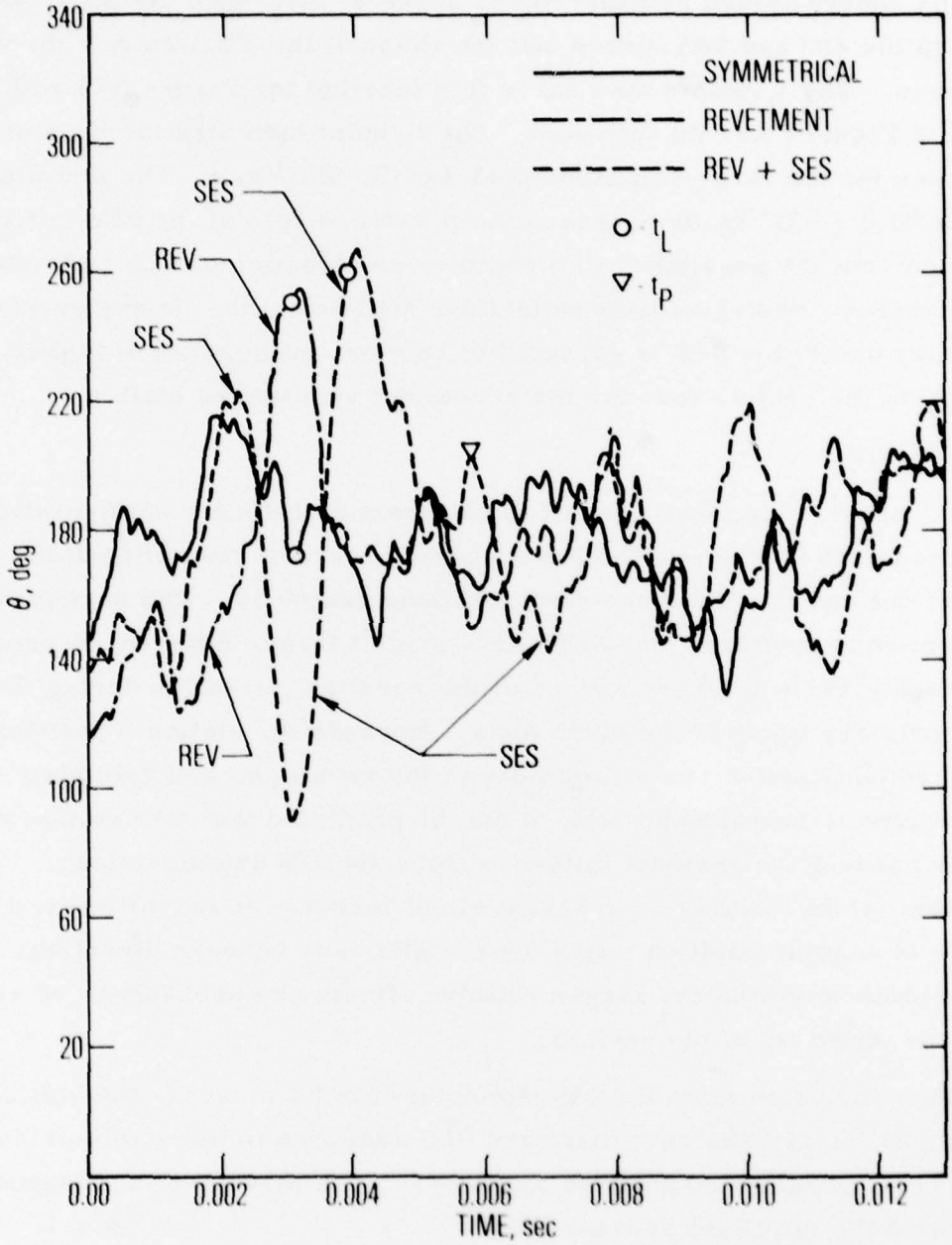

Figure A-5. Time History of Pressure Differential Direction

The superimposed symbols for t_L serve to reference the peaks and valleys in the r(t) and θ(t) curves and the shape of the Figures A-1 through A-3 curves. The t_t points also serve this function for Figure A-4 with respect to Figures A-1 through A-3. The t_p point indicates the time of occurrence for the large amplitude peak for the SES case. The simultaneous direction of θ = 205° tends to lessen the presumed role of the SES in its production, but the possibility of a complex combination of SES reflections, flow convection, and revetment reflections still remains. In any event, the asymmetry due to the SES is expected to be more pronounced at higher positions on the vehicle than for the revetment surrounded station 3.

CONCLUSIONS

The shock-tube simulation of the Minutemen I RSLP* configuration launch transient flow does exhibit noticeable pressure force magnitude and direction changes for the three configurations examined. The asymmetrical revetment and revetment plus SES cases exhibit larger differential pressures force magnitudes and larger swings of the resultant direction during the test time of primary interest for these tests. Because the station 3 positions considered here are in close proximity to the revetment and relatively far from the (downstream) SES walls, it can be predicted that this station will probably not feel the greatest influence from the SES asymmetries. Therefore, while there is an apparent slight increase in magnitude and large increase in angular position swing for the SES case between directions of SES maximum asymmetry, larger relative effects are probably to be seen nearer the upper tip of the vehicle.

The conclusion from the experimental data (at least for the station 27.5 output), is that the revetment and SES additions to the symmetrical silo exit configuration do produce increases in the magnitude and angular variation of the resultant pressure force.

*RSLP = Reentry System Launch Program

APPENDIX B

APPLICATION OF COORDINATE TRANSFORMATION TO TDV-3 FULL-SCALE FLIGHT DATA

Appendix A contains a description of how the rectangular coordinate pressure-difference-force component time histories could be combined into a vector magnitude and direction pair of signatures in polar coordinates, and a new viewpoint for considering the effects of these forces was thereby established. It is realized that the data reduction and analysis technology represented by the digital computer programs developed for the shock-tube tests could also be applied to the full-scale test data from the Vandenburg AFB launches when equivalent information is available from them.

The TDV-3 launch in November 1977 was the first test for which four pressure transducers were incorporated at a single upper vehicle axial station (RAW* section), rather than the single pair employed for a few previous launches. In addition, the two radial accelerometers at the same axial station and azimuthal alignment yielded a pair of rectangular coordinate components of the total local lateral acceleration vector time histories that could be combined by the same coordinate transformation as used for the pressure differences, to give a total acceleration-response vector signature. Thus, the relationship between the time histories of the pressure-difference forces (input) and the acceleration (response) at the RAW section could be compared for insight into the degree of correspondence between them. The remainder of this appendix describes the application of the previously developed subscale data reduction techniques to the TDV-3 data, and an evaluation of the signature comparison for that launch.

EXPERIMENT DEFINITION

The data treated come from transducers mounted in the RAW section (axial station 164) of the Minuteman I (MMI) RSLP TDV-3 launch. The

*RAW = Retro Adapter Wafer

transducers are four ported pressure (acoustic) transducers mounted at vehicle azimuths of 0, 90, 180, and 270°, and two radial accelerometers with sensitive axes aligned with the 0 to 180° and 90 to 270° diameters. The data is telemetered to a ground receiver on FM/FM Link 35 and the various frequency multiplexed subcarrier channels are predetection recorded on a wideband instrumentation magnetic tape recorder. The 0° pressure information is on channel F, 90° on B, 180° on H, and 270° on D. The 0 to 180° accelerometer output is transmitted on channel 12, and the 90 to 270° on channel 13.

The time interval of interest begins just before motor ignition and continues for about 1/4 to 1/2 second. This interval includes the ignition transient, the arrival of the N-wave at the RAW section, range liftoff signal, and the return of the pressure fluctuation levels to the lower amplitudes characteristic of the time period after passage of the N-wave.

DATA REDUCTION

The original data is contained in analog format on the Link 35 telemetered FM/FM frequency multiplexed (subcarrier) magnetic instrumentation tape. These data, contained in channels 12, 13, B, D, F, and H, are demodulated with the aid of EMR type 4142 tunable discriminators. The discriminator low pass filter (7-pole) is set to CD (constant delay, linear phase, or Bessel) characteristic to preserve waveform fidelity, and the cutoff frequency set to a value appropriate to channel information bandwidth. The time-dependent discriminator output is passed through an analog-to-digital conversion process and an FM calibration program, the result being a calibrated digital standard data tape.

The pressures at 0, 90, 180, and 270° (scalars) are differenced to give the appropriate x and y gradients (vectors). The original pressure waveforms, the differences, and the x and y accelerations are Calcomp plotted after appropriate digital filtering. These results have also been obtained for prior tests.

The new element in the data reduction process reported in this memorandum is the transformation of the x, y (or orthogonal) representation to an r, θ (vector magnitude, vector direction) representation. This polar coordinate transformation is shown in Figure B-1. The standard vector identities between orthogonal and polar coordinates pertain, with the $x = x(t)$, $y = y(t)$, $r = r(t)$ and $\theta = \theta(t)$ being continuous time series variables and the physical dependent variable being either pressure difference or acceleration, as required. The angular coordinate is the launch azimuth in vehicle coordinates, where the launch direction defines 0°, and the clockwise increasing angle, as shown in the figure, is obtained by viewing upward from the bottom or nozzle end of the vehicle.

Calcomp plots of vector magnitude (r) and vector direction (θ) are obtained to show the time signature of both of these parameters for the excitation (pressure differential force) and the response (acceleration). In order to show the main features of these traces, stronger digital filtering (lower cutoff frequency) was applied in some cases. In order to allow the digital filtering process to give the expected filter function at these very low filter cutoff ratios, it was necessary to thin the sample ensemble by selecting a new sample set made up of every tenth point of the original sample set. The definition of filter cutoff frequency, for all digital filtering considered in this report, is the frequency for which the filter function amplitude drops to one-half of the unattenuated amplitude.

RESULTS AND DISCUSSION

The results of this investigation are displayed by the computer output Calcomp plot Figures B-2 through B-5. Each figure presents the excitation of Δ pressure trace in the upper half, and the response or acceleration in the lower half, each on a common time base. The results for both vector magnitude and vector direction are presented for cases where the data has been digitally low-pass filtered to 75 Hz and 25 Hz. These frequencies were selected, in part, because of an assumption that, in some approximate

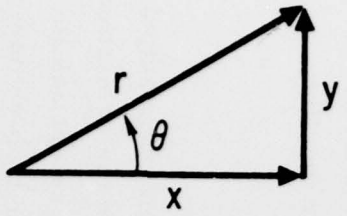

$$r = \sqrt{x^2 + y^2}$$

$$\theta = \tan^{-1} \frac{y}{x}$$

$$x = x(t) = \ddot{x}(t)_{0\text{-}180} = \Delta p(t)_{0\text{-}180}$$

$$y = y(t) = \ddot{y}(t)_{90\text{-}270} = \Delta p(t)_{90\text{-}270}$$

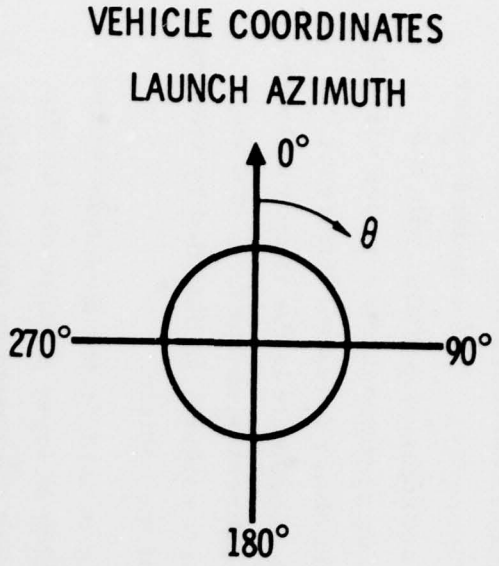

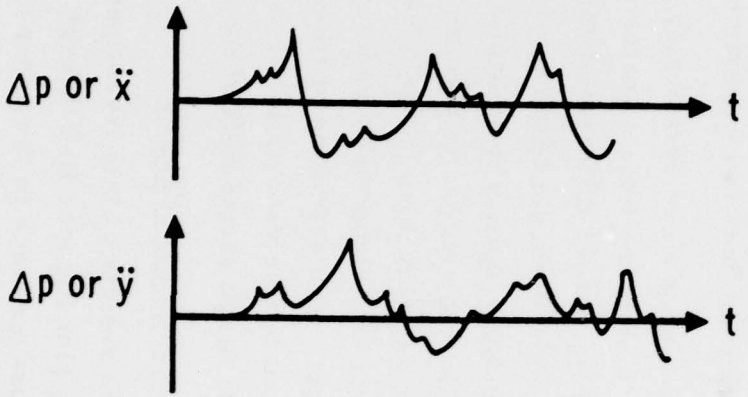

Figure B-1. Polar Coordinate Transformation

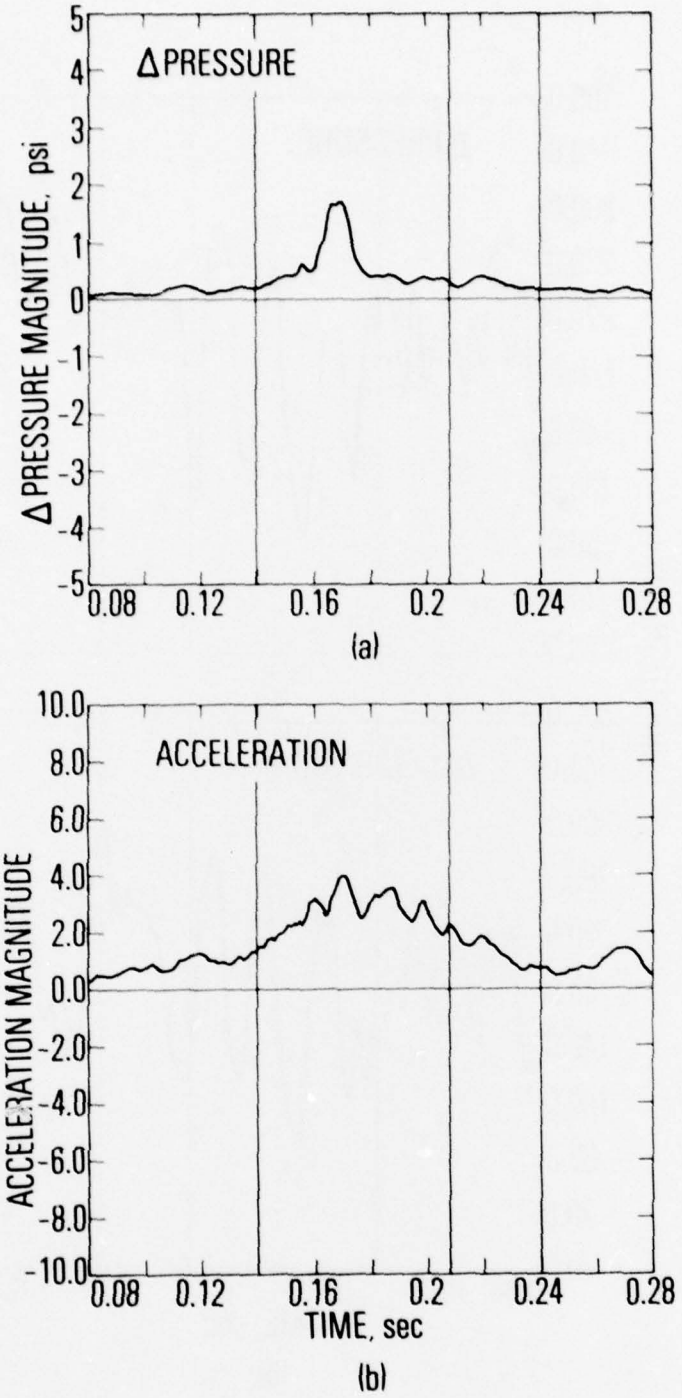

Figure B-2. Comparison of Vector Magnitude for (a) Pressure Differential and (b) Acceleration Measured at Upper Vehicle RAW Section for TDV-3 Launch. 75-Hz filter.

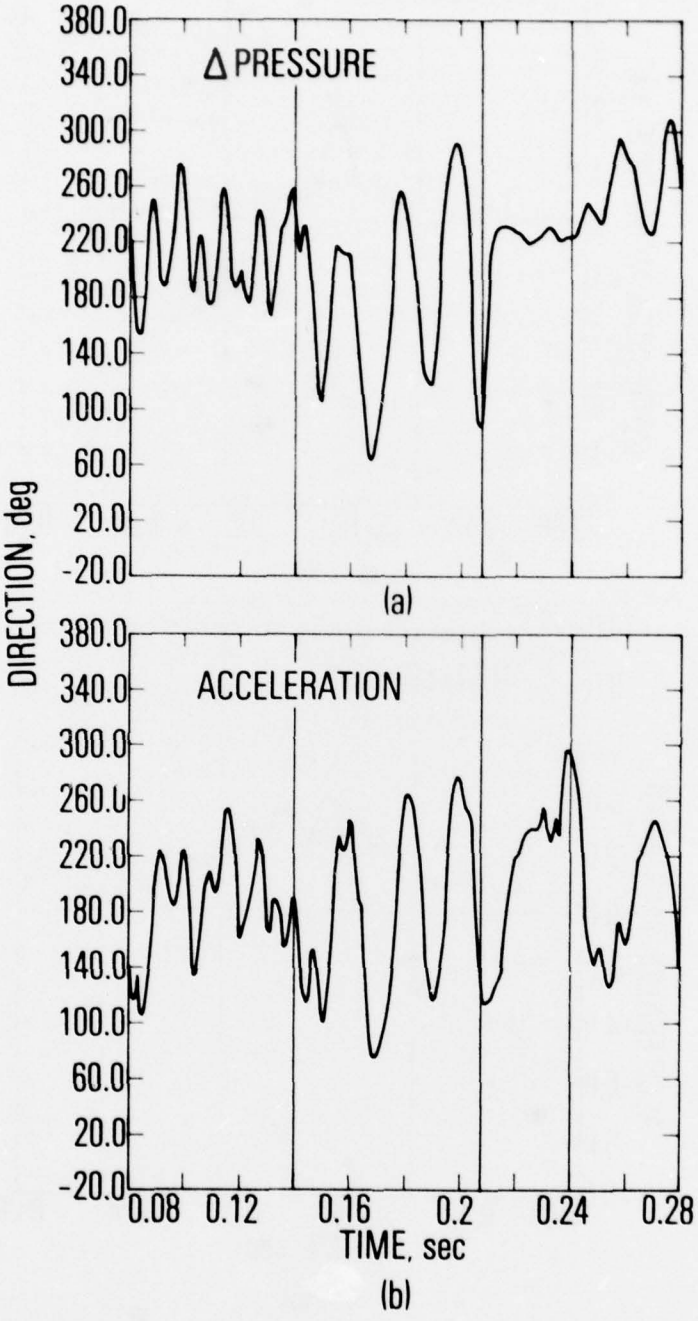

Figure B-3. Comparison of Vector Direction History at Upper Vehicle RAW Section for TDV-3 Launch. (a) ΔPressure; (b) Acceleration. 75-Hz filter.

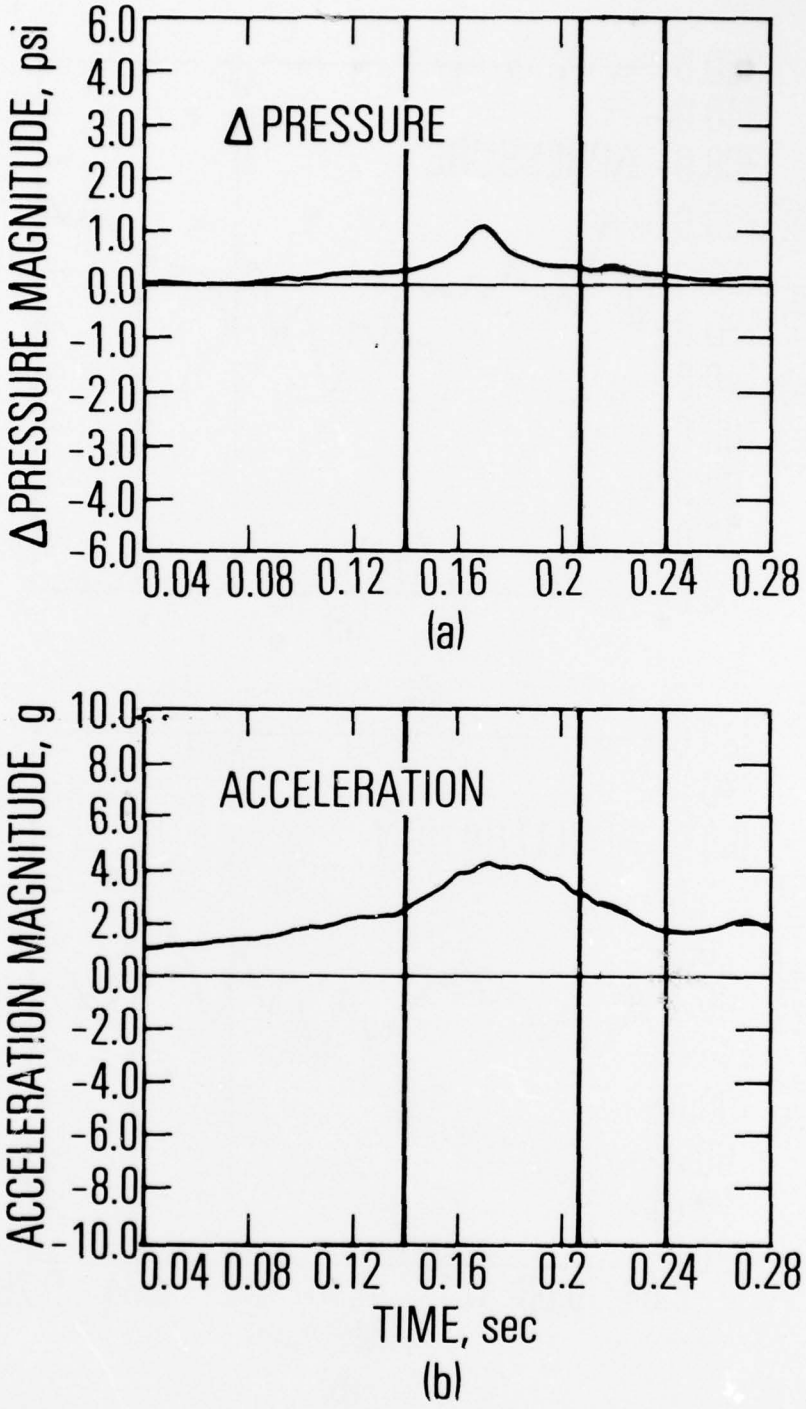

Figure B-4. Comparison of Vector Magnitude for (a) Pressure Differential and (b) Acceleration Measured at Upper Vehicle RAW Section for TDV-3 Launch. 25-Hz filter.

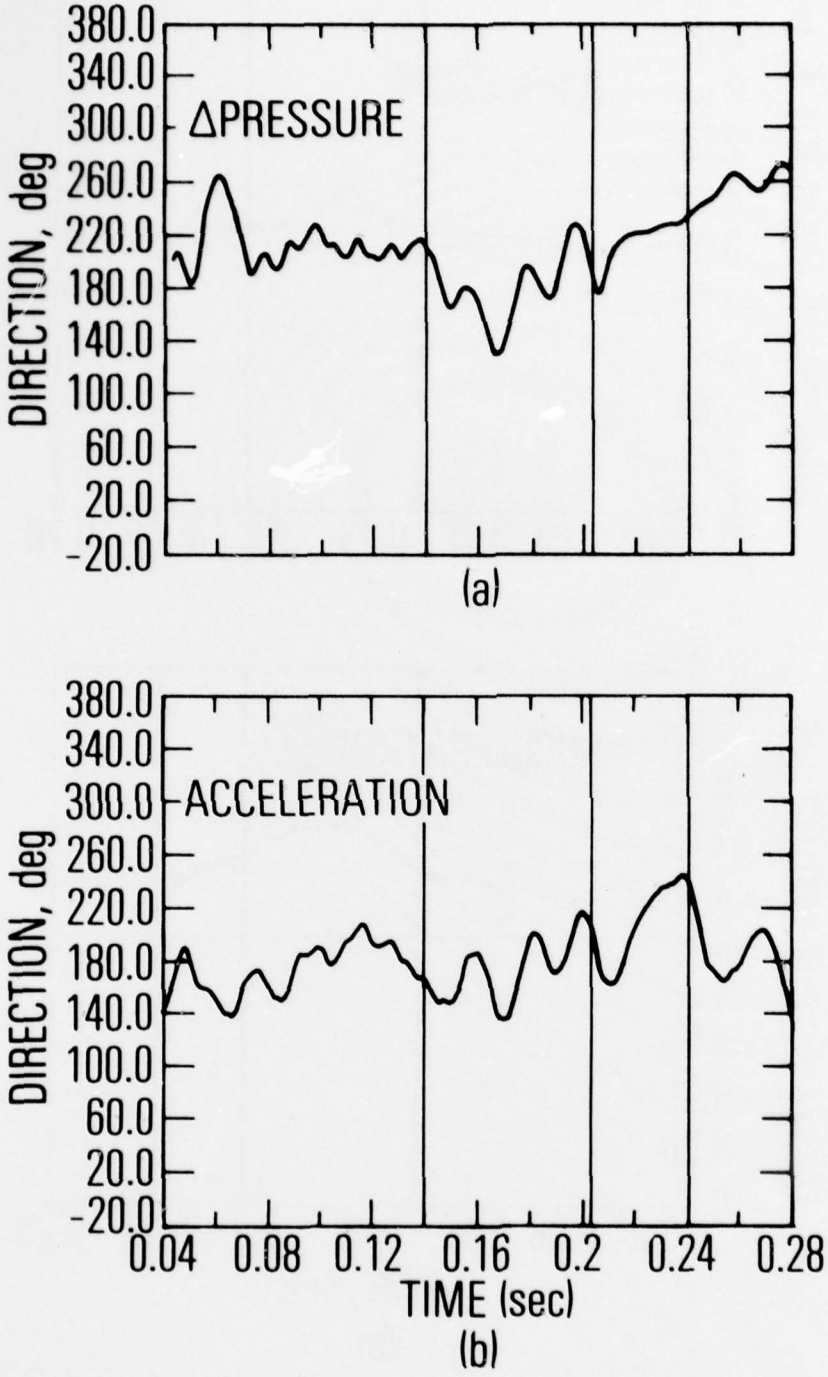

Figure B-5. Comparison of Vector Direction History at Upper Vehicle RAW Section for TDV-3 Launch. (a) ΔPressure; (b) Acceleration. 25-Hz filter.

sense, these frequencies are representative of the range responsible for significant loads in the structure. A more precise evaluation of the significant structural load frequency range awaits the results of studies of cumulative modal load contributions being carried on by Boeing and The Aerospace Corporation.

The common time zero represents 0815.00.08 Z time or Greenwich Mean Time. The three solid vertical lines are for reference purposes. The line at 0.208 sec represents the nominal reported range "liftoff time" of 0815.01.008 Z. The other two lines include a period where the excitation value of $\Delta p > 0.5$ psi is deemed "significant." This time period from 0.14 to 0.22 sec is also the approximate duration of the N-wave signature at each of the four pressure transducers. For reference purposes the "ignition time" is at about 0.038 sec on the left-hand edge of the Calcomp trace; and the arrival of the pressure waves at the (station 164) pressure ports is at 0.08 sec.

Both the pressure and acceleration measurements are made at the same nominal axial location, station 164. It is expected that the local Δp force would have a major role in determining the acceleration response, but the response is also subject to any other forces on the vehicle. These forces produce rapidly propagated stress waves within the structure and can contribute to the sensed acceleration. The forces include any unbalanced pressure forces acting on the entire axial extent of the vehicle, from ignition transient forces, from nozzle flow separation forces, etc. If there is reasonable correspondence in the time signature of the Δp and acceleration functions within the time period of interest (within the boundary lines), then a reasonable spatial coherence of the Δp forces over some extended region of the vehicle in the neighborhood of the pressure ports, as well as the measurement point, is assumed.

In the vector magnitude 75-Hz filter case, Figure B-2, the general character of the two functions is the same, but the duration of the Δp pulse

is less than that of the acceleration. This behavior is reasonable when consideration is given to the fact that force inputs from other axial stations can be felt at station 164. The Δp peak of 1.7 psi is followed a few milliseconds later by an acceleration peak of 4.0 g.

Figure B-3 presents the related story of vector direction with 75-Hz filter. The general similarity of the input and response direction-time histories in the interval of interest is remarkable. The traces from 0.08 to 0.14 sec are also in general agreement. The remarkable correspondence between about 0.15 to 0.23 sec for the two traces is shown by the nearly sinusoidal character with about 50-Hz frequency and 180° amplitude, and with a mean value increasing (with increasing time) between about 140° and 200°. The acceleration trace is delayed by about 2 to 3 msec with respect to the Δp trace. The close similarity of the directional signatures within this time period is advanced as the most significant result of this investigation.

Similar behavior is displayed by the 25-Hz filtered versions of the vector magnitude (Figure B-4) and vector direction (Figure B-5). The amplitude of both the magnitude pulse and the angular excursions are reduced when compared to the 75-Hz filter case, but the same general behavior and correlation between the traces is observed in a smoothed out version.

One aspect of the r-θ presentation determined worthy of future study is the apparent simplicity of possible analytical approximations to both the r and θ components when contrasted to the two orthogonal representations of the same phenomena. This might prove useful in developing the final MMI RSLP Lateral Load Forcing Function Model.

One very simplified conceptual model of the load producing action is provided by a rectangular (or constant) magnitude function and a sinusoidal non-constant-mean direction function over the time interval previously discussed.

No attempt will be made in this appendix to back out the influence of the launch facility geometrical asymmetries in generating the observed signatures due to both the oscillatory character of the result and the lack of alignment with a given asymmetry. These asymmetries include at least those in the vicinity of the silo exit, the SES, the revetment asymmetry, and the umbilical tower and other ancillary structural elements. It is probable that a complex interaction between these geometrical asymmetries and such features of the flow as wave reflections, the transient starting ring vortex at the silo exit, and the quasi-steady sonic or supersonic annular jet flow is responsible for the observed behavior.

CONCLUSIONS

The major conclusions of this investigation are as follows:

1. The r-θ presentation of Δp and acceleration allow additional insight into the launch transient process not easily perceived from the orthogonal or x-y presentation. The already developed techniques discussed herein should be applied to all future RSLP launches where bi-axial data is available. Application to selected prior data should be considered.

2. There is generally good agreement between the local RAW station 164 Δp and acceleration magnitude histories. There is remarkable agreement between the respective directional signatures during the period when their magnitudes are significant.

3. Substantial, coherent oscillation of both the Δp and acceleration vectors occurs during the significant magnitude time interval, with an approximate frequency of 50 Hz and a magnitude of 180° (when conditioned by a 75-Hz filter).

4. The observed time coherency implies substantial spatial coherency of the Δp forces over some reasonable axial extent of the vehicle in the neighborhood of the RAW section (station 164).

5. The strong correlation between the directional histories of upper vehicle Δp and acceleration implies a similarly strong basis for the hypothesis that these upper vehicle Δp forces constitute the major contributor to the upper vehicle lateral loads during the MMI RSLP launch transient.

6. When comparing the pressure force direction signature for the shock-tube and TDV-3 cases, similar behavior with sinusoidal oscillation in the range of about 50 to 60 Hz (referred to full scale by model time scale factor) is observed for both. There are about 4 cycles for TDV-3 and 1-1/2 cycles for the model. TDV-3 was flown with an SES on top of the silo, and the SES installed model case was used for comparison.